國立臺灣大學電機資訊學院生醫電子與資訊研究所

博士論文

Graduate Institute of Biomedical Electronics and Bioinformatics

College of Electrical Engineering and Computer Science

National Taiwan University

Doctoral Dissertation

慢性中風病人接種幹細胞後以磁振造影追蹤及測量灌流變化的應用和限制

Applicability and limitations of MR tracking and Perfusion change after intracerebral stem cell Implantation in chronic stroke patients

林昭君

Chao-Chun Lin

指導教授: 鍾孝文　博士

Advisor: Hsiao-Wen Chung, Ph.D.

中華民國 102 年 7 月

July, 2013

論文致謝：

有機會寫這篇感謝文，首先要提沈戊忠院長，在我第一年考上博班時無條件支持我唸書，如果隔一年再唸，有可能沒有一鼓作氣的熱情了。再來是在博一到博二，一星期要南北來回三天，博三一星期兩天，幾乎有一半的工作天都在台北，同事羅于倩醫師無怨無悔的幫忙支援我的工作，蔡伯邦醫師幫忙打plain film，讓我的報告可以不至於看不到盡頭，也才能在每個晚上和假日完成所有的報告。阮春榮醫師是我學習的目標，因為有他成功的走在前面，我才有勇氣走下去，他也毫不吝惜於提供個人的心得，提供很多博班的攻略。沒有林欣榮院長和徐偉成院長的臨床試驗，就沒有這篇論文，非常感謝他們的耐心和包容。

感謝鍾孝文老師及實驗室裡眾多優秀的學長姐，這是台灣MRI最好的智囊團。不過入寶山能挖多少寶藏而回，其實是端看個人的努力，雖然我只能窺得寶山的一隅，但是已經盡力了。感謝鍾老師提醒我很多無形的寶貴課程，包括耐心和團隊合作。劉益瑞學長一直提供很多在課業和實驗上的幫忙，沒有他， 我應該撐不到最後，雖然中間有點小插曲，非常感謝他不計前嫌，很寬容的理解和包容，也非常謝謝他一路陪我成長。慶昭非常聰明，總是可以很快的理解我的實驗上的需求和問題，且提供GE機器上最好的解決方案。吳文超學長是我MR perfusion部份能有小小結論的大功臣，一開始失敗時，kk學長提供了很好的建議，另外有很多小細節，也都是有賴於他的解答和分析，他總是很熱心且有

耐心的回答我的問題。身為在職生，常不在實驗室，感謝正傑和學弟妹們很熱心的幫忙很多小細節。

感謝小媽在病人檢查時間安排上的幫忙，讓資料收集很順利。家瑋是個做事很認真確實的同事，感謝他犀利的眼睛，在一開始資料收集最重要的階段，讓資料因不同次檢查而造成的誤差減到最小。巧穎是個很有耐心且細心的幫手，在資料分析階段是個任勞任怨的好助手。曉微在小磁珠分析階段提供了很多的幫忙。

感謝媽媽每個周六的陪伴，幫我料理家務。Mimi, Lulu 和多多三隻小天使溫馨的陪伴。還有孝貞的鼓勵，佩曄無條件的支持陪伴，和加油，這些都是我可以撐到最後最重要的動力。

像 MRI 一樣，要 SNR 高，時間就要長，時間要縮短，就可能犧牲掉影像品質，想兼顧臨床工作和研究，是一件很貪心的事，結果變成兩者都做不好。MRI 的定量分析真的是需要大量的時間做看似簡單的圈 ROI 工作，好不容易圈完了，統計沒有意義，又要再重來一次，就算有意義，也要除錯，看是不是真的有意義，還是分析方法錯誤，這樣的苦工，技術性說高不高，但是要很有耐心，還有團隊的支援，才得以完成這樣一件小小的成果，雖然成果看似不起眼，可是一晃眼已經過了五年。「An expert is a man who has made all the mistakes which can be

made, in a narrow field」-by Niels Bohr. 這五年我在一個很小的領域裡犯了很多的錯誤，感恩所有幫忙的人。

最後，感謝口試委員劉金昌副院長，陳啟昌主任，郭萬祐主任，以及高怡宣教授的意見和指教。

中文摘要

中風為 2010 年台灣第三大死因，但目前尚無任何讓慢性中風病人神經再生的治療方法。有越來越多的動物研究顯示，幹細胞將是中風未來一個嶄新的治療。在本院臨床二期試驗中，我們將大腦周邊血液的造血幹細胞($CD34^+$)植入慢性中風患者腦內，並運用 MRI 非侵入性的特點，以 $R2^*$弛緩率觀察被超順磁性氧化鐵顯影劑標幟之植入幹細胞。

由動物研究推測，$CD34^+$細胞能誘導缺血區的血管新生，此發現推測在神經再生中扮演重要角色。因此，我們希望以 $T2^*$灌流序列量測慢性中風病人在接種幹細胞前後的腦血流改變，證明腦血流速及腦血流量增加與幹細胞移植的相關性。

關鍵字：

$CD34^+$細胞、慢性中風、灌流磁振造影、$R2^*$弛緩率、幹細胞

Abstract

Stroke is the 3rd leading cause of death in Taiwan on 2010. In the chronic stage, no treatment currently exists to restore lost neurological function after stroke. A growing number of studies highlight the potential of stem cell transplantation in animal model as a novel therapeutic approach for stroke. One phase II clinical trial in our institution studied the therapeutic effects with intracerebral peripheral blood hematopoietic stem cell ($CD34^+$) implantation for chronic stroke patients. This regular MRI follow-ups are aimed to noninvasively monitor the fate, behavior of the implanted stem cells labeled with superparamganetic iron oxide by $R2^*$ relaxivity. Besides, since animal studies hypothesize that $CD34^+$ cells may play a positive role in neuroregeneration by inducing neovascularization in the ischemic zone, we want to test the hypothesis of increased cerebral blood flow and volume associated with stem cell implantation, also by MR $T2^*$ perfusion sequence.

Key words:
$CD34^+$ cell, Chronic stroke, MR perfusion, $R2^*$ relaxivity, stem cell

Table of Contents

List of Figures

Chapter3

Longitudinal perfusion change after intracerebral CD 34^+ stem cells implantation in chronic stroke patients

List of Tables

Chapter 1

1.1 Stroke in Taiwan

Stroke is the 3rd leading cause of death in Taiwan, behind cancer and heart disease. The prevalence of stroke in Taiwan was 1.64% (1). Despite the high mortality, about 17,000 stroke patients survive with moderate to severe disabilities each year in Taiwan (2). The direct and indirect annual expenditure on stroke in Taiwan is estimated to be 40 billion which is the top 3 expenditure from National health insurance (2).

A stroke is a condition in which the brain cells suddenly die because of a lack of oxygen. This can be caused by an obstruction in the blood flow, or the rupture of an artery that feeds the brain. The distribution of stroke subtypes included ischemia (67.1%), hemorrhage (14.0%), subarachnoid hemorrhage (4.2%), and unclassified type (14.7%)(1).

1.2 Current stroke treatment

In the hyper-acute stage of stroke, CT or MR perfusion imaging serve an important role in identifying potentially salvageable tissue at risk (penumbra) (Figure 1.1). Treatment with “clot-busting” tissue plasminogen activatior (tPA) administered within 3h of the onset of ischemia is currently the only accepted treatment for ischemic stroke. In

the acute stage (within days after infarct), stabilization of vital signs and intracranial pressure is important in patients with neuronal death and neurological deficits. If the patients survive from the stroke with stable condition and neurological deficits, rehabilitation can improve the behavior compensation and physiological plasticity.

1.3 Plasticity of cortical projections after stroke

Endogenous recovery after stroke involved at least three processes: resolution of acute tissue damage, behavioral compensation, and neuroplasticity (Figure 1.1). Initial improvements in neurological function occur during the acute stage of stroke, within days of the infarct. Late improvements in function occur through behavioral compensation weeks to months after infarct. Between the resolution of acute tissue damage and the late behavioral compensation, stroke induces profound changes in cortical circuits. This post stroke neuroplasticity includes alterations in the structure and physiology of cortical connections (3-6). In one animal study (6), data by immunohistochemistry methods support the neurite growth followed by synaptogenesis in the neocortex in a pattern that corresponds both spatially and temporally with behavioral recovery. However, the endogenous mechanisms of neural repair lead to

only limited functional recovery (5) and the repair is most active in the first 2 months (5-6).

Figure 1.1. The pathologic changes, neurologic deficits and treatment in different stages of middle-cerebral-artery infarction

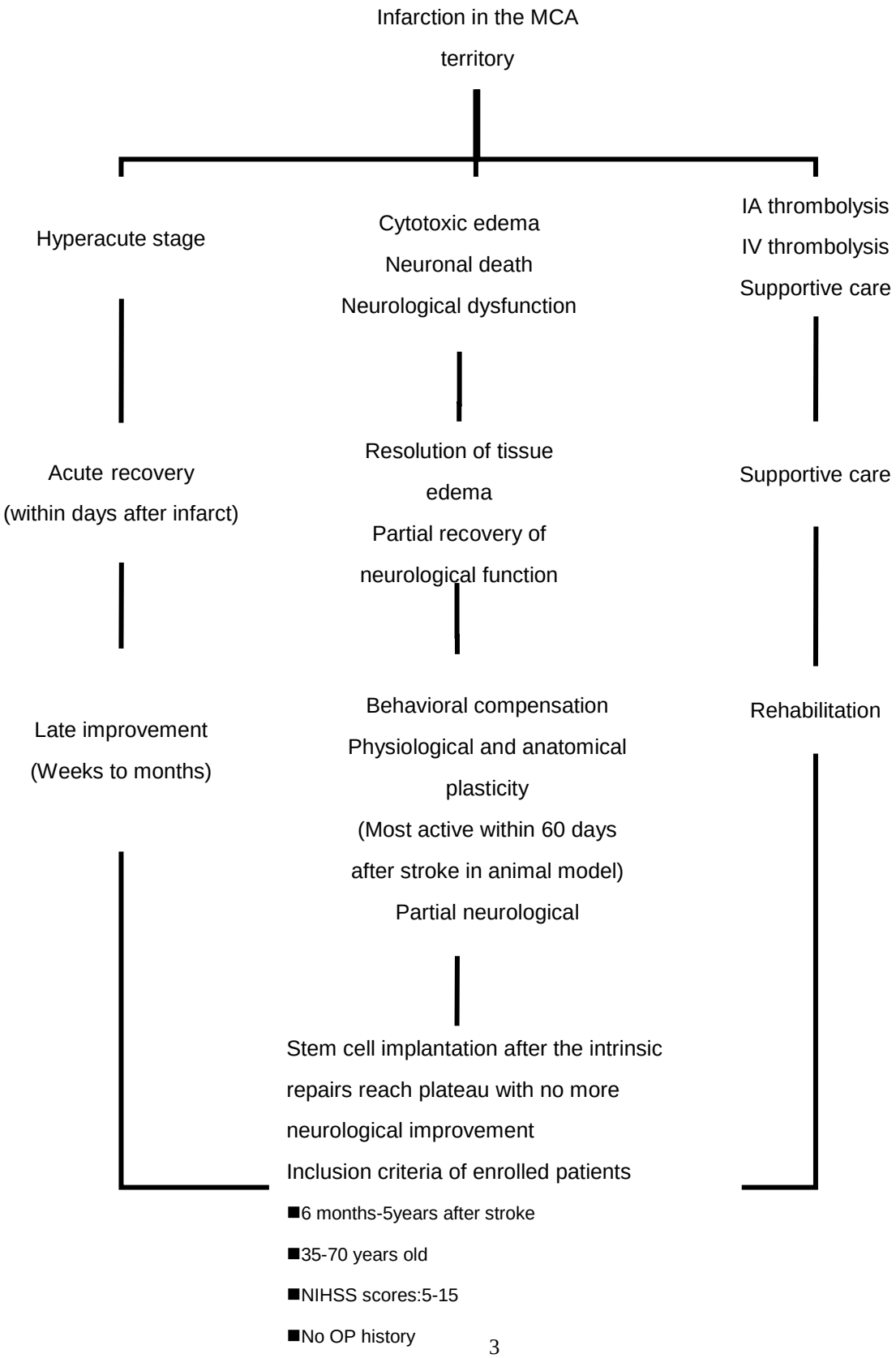

1.4 Stem cell-mediated brain repair for stroke

A growing number of studies in animal model highlight the potential of stem cell transplantation as a novel therapeutic approach for stroke. Despite unclear underlying mechanisms of transplanted cell-mediated recovery, improvement of various stroke-induced behavioral deficits has been observed in many animal studies (7-16). A variety of cell types derived from humans have been tested in experimental stroke models. They fall into 3 categories: 1) neural stem/progenitor cells (NPCs) cultured from fetal tissue; 2) immortalized neural cell lines; and 3) hematopoietic/endothelial progenitors and stromal cells isolated from bone marrow, umbilical cord blood, peripheral blood, or adipose tissue. Among these, human bone marrow cells, human umbilical cord blood cells, peripheral blood progenitor cells, and adipose tissue mesenchymal stem cells have been reported by several groups to enhance functional recovery, whether delivered intracerebrally or intravenously (8-10, 14-15). The advantages of a hematopoietic source of cells are 1) they avoid the ethical issues and tissue limitation associated with embryonic and fetal tissue. 2) Human bone marrow cells and peripheral blood stem cells also offer the potential of autologous transplants, negating the need for

immunosuppression regimens. 3) These cells are already used in the clinic for various malignant and nonmalignant disorders (17). 4) The use of human umbilical cord blood cells for traumatic brain injury in children has just been approved; this is the first clinical trial using these cells for a neurological disorder. In one animal study, rats receiving intracerebral peripheral blood hematopoietic stem cell ($CD34^+$) (PBSC) transplantation showed much more improvement in neurological function after chronic cerebral ischemia in comparison with vehicle-treated control rats (15).

1.5 Potential mechanisms of transplanted cell-mediated recovery

1) Integration into the host circuitry

In rat studies, the stroke rat with behavioral recovery can be observed with only a few cells surviving or integrating after transplantation (11-12, 18). However, evidence for this is limited. Besides, the small numbers of transplanted cells surviving in the post stroke brain reported in some studies (11-12) may pose a major problem if integration into the host circuitry is necessary for improved neurological outcome.

2) Attenuation of inflammation

An intriguing potential repair mechanism is the ability of transplanted cells to attenuate the stoke-induced inflammatory/immune response.

Intravenous injection of human umbilical cord blood cells reduced leukocyte infiltration into the brain (19), although it is not clear whether this is a direct effect on the inflammatory response or a secondary effect attributable to a reduction in infarct size (17).

3) Transplanted cells reduce death of host cells.

Acute delivery of cells often reduces lesion size and inhibits apoptosis in the penumbra, suggesting that enhanced recovery results from neuroprotection. The secretion of trophic factors, such as vascular endothelial growth factor, fibroblast growth factor, glial cell-derived neurotrophic factor, and brain-derived neurotrophic factor, is likely to contribute to this neuroprotective mechanism (20-22).

4) Induction of host brain plasticity

An increase in endogenous brain plasticity and motor remapping after ischemia is postulated to underlie the spontaneous recovery seen after a stroke (4-6). Cell transplantation may enhance these endogenous repair mechanisms. Shen et al (14) reported that bone marrow stromal cell treatment markedly increased vessel sprouting, synaptophysin expression and oligodendrocyte precursor cells in the corpus callosum. These results suggest that bone marrow stromal cells facilitate axonal sprouting and

remyelination in the cortical ischemic boundary zone and corpus callosum.

5) Increased neovascularization

Transplanted cell-induced blood vessel formation has been reported with bone marrow stromal cells (10, 14), neural stem cells (23), and cells from human cord blood and peripheral blood (15). Human CD 34^+ cell also have been shown to enhance neovascularization at the border of the ischemic zone followed by endogenous neurogenesis (24).

6) Recruitment of endogenous progenitors

Endogenous neurogenesis is increased after a stroke (25). The function of this has yet to be determined but may signify a natural repair mechanism of the brain that could potentially be further enhanced by transplanted cells. There is precedence for this with cord blood cells and bone marrow cells (24, 26).

1.6 Current clinical trials involving stem cells as stroke therapy

Do the data from animal experiments give a true indication that stem cells might be effective in clinical trials? Currently, stem cell therapy in stroke patients is in its infancy. Table 1 summarizes current clinical trials involving stem cells as stroke therapy (27). These small initial human

studies are hardly to be comparable due to differences in type of cells, timing of injection and mode of delivery. The initial human studies indicate that stem cell therapy may be technically feasible in stroke patients, but the efficacy has not been proven in humans (28-30). One phase II clinical trial in our institution aimed to evaluate the effect of autologous CD 34^{+} stem cell implantation for chronic stroke patients. The patients enrolled in this clinical trial received regular MRI follow-ups. Our study aims to noninvasively monitor the fate, behavior of the implanted stem cells labeled with superparamganetic iron oxide by $T2^{*}$-weighted MR imaging. Besides, since animal studies hypothesize that $CD34^{+}$ cells may play a positive role in neuroregeneration by inducing neovascularization in the ischemic zone, we want to test the hypothesis of increased cerebral blood flow associated with stem cell implantation, also by MR $T2^{*}$ perfusion sequence.

Table 1.1 Current clinical trials involving stem cells as stroke therapy

Title of trial	Inclusion criteria	Intervention	Outcome/status
Efficacy study of CD34 stem cell in chronic stroke	Ischemic stroke in MCA territory (6-60 mo); NIHSS 9-20; 35-70 y; M+F	Intracerebral implantation of 2–8 × 10^6/patient autologous $CD34^+$ cells (hematopoietic progenitors), plus conventional stroke therapy[a]	Completed (phase II)
fMRI in monitoring intracerebral stem cell implantation for chronic stroke patients	Ischemic stroke in MCA territory (0.5–3 yr); NIHSS 9–20; 35–75 yr; M + F	Intracerebral implantation of hematopoietic stem cells; remyelination, increased perfusion, and cortical activity in penumbra observed using fMRI	Completed
Pilot investigation of stem cells in stroke	Unilateral ischemic stroke (0.5–5 yr); NIHSS >6; 60–85 yr; M only	Intracerebral injection of 2/5/10/20 × 10^6/patient ReNeuron CTX0E03 neural stem cells	Recruiting (phase I)
A study of modified stem cells in sable ischemic stroke	Ischemic stroke in subcortical region of MCA or lenticulostriate artery (with or without cortical involvement; 6–24 mo); NIHSS >7; 18–75 yr; M + F	Intracerebral implantation of 2.5/5/10 × 10^6/patient modified stromal cells (SB623)	Recruiting (phase I/IIa)
Study of purified umbilical cord blood $CD34^+$ stem cell on chronic ischemic stroke	Ischemic stroke (6–60 mo); NIHSS 5–15; 35–70 yr; M + F	Intercerebral implantation of allogenic $CD34^+$ stem cells produced from StemCyte umbilical cord blood	Not yet recruiting
Implantation of Olfactory ensheathing cells (OECs)	Ischemic stroke in MCA territory (6–60 mo); NIHSS 5–15; 35–70 yr; M + F	Autologous OECs cultured before treatment; intracerebral implantation of 2–8 × 10^6/patient OECs	Recruiting (phase I)
Autologous bone marrow stem cells in middle cerebral artery acute stroke treatment	Acute ischemic stroke in MCA territory (5–9 d); NIHSS >8; 18–80 yr; M + F	Intra-arterial implantation of autologous $CD34^+$ cells *via* MCA	Completed
Study of autologous stem cell transplantation for patients with ischemic stroke	Ischemic stroke in MCA territory (3–90 d); NIHSS 4–20; 18–75 yr; M + F	Intra-arterial or intravenous injection of 500^6/patient autologous bone marrow stem cells	Completed
Autologous bone marrow stem cells in ischemic stroke	Acute total anterior circulation ischemic stroke (<7 d); NIHSS severe; 30–80 yr; M + F	Intra-arterial implantation of autologous $CD34^+$ cells *via* MCA	Recruiting (phase I/II)
Study to assess the safety and effects of autologous adipose-derived stromal cells in patients after stroke	Ischemic stroke or hemorrhagic stroke; NIHSS ≧8; 18–80 yr; M + F	Internal Carotid Artery and intravenously injection of adipose-Derived Stromal Cells (ASCs)	Recruiting (phase I/II)
Study of ALD-401 *via* intracarotid infusion in ischemic stroke subjects	Ischemic stroke in MCA territory (11–17 d); NIHSS ≧4; 30–75 yr; M + F	Intracarotid injection of ALD-401 autologous bone marrow stem cells	Recruiting (phase II)

Study to assess the safety and effects of autologous adipose-derived stromal cells in patients after stroke	Hemorrhagic or ischemic stroke; NIHSS >8; 18–80 yr; M + F	Intracarotid or intravenous administration of autologous adipose-derived stromal cells (cells isolated and delivered within 1 h)	Recruiting (phase I/II)
Intravenous autologous bone marrow-derived stem cells therapy for patients with acute ischemic stroke	Ischemic stroke (7–30 d);NIHSS >7; 18–80 yr; M + F	Intravenous injection of 30–500 × 10^6 autologous bone marrow-derived mononuclear cells	Completed (phase II)
Intravenous stem cells after ischemic stroke (ISIS)	Acute carotid ischemic stroke (<14 d); NIHSS 2–24; 18–85 yr; M + F	Intravenous injection of autologous MSCs <6 wk after stroke	Recruiting (phase IIa)
A study of allogeneic mesenchymal bone marrow cells in subjects with ischemic stroke	Ischemic stroke (>6 mo); NIHSS 6–20; >18 yr; M + F	Intravenous injection of 0.5–1.5 × 10^6/kg autologous MSCs <6 wk after stroke	Recruiting (phase I/II)
Autologous bone marrow stromal cell and endothelial progenitor cell transplantation in ischemic stroke	Ischemic stroke in MCA territory (7 d); NIHSS ≧7; 18–80 yr; M + F	2 times intravenous transplantation of 2.5 × 10^6 bone marrow stromal cells or endothelial progenitor cells/kg	Recruiting (phase I/II)
Intravenous Autologous mesenchymal stem cells transplantation to treat middle cerebral artery infarct	Ischemic stroke in MCA territory; NIHSS 10–30; 30–70 yr; M + F	Intravenous autologous bone marrow-derived mesenchymal stem cells	Recruiting (phase II)
Safety/feasibility of Autologous mononuclear bone marrow cells in stroke patients	Ischemic stroke (24–72 h); NIHSS 6–15(R)/18(L); 18–80 yr; M + F	Intravenous injection of autologous mononuclear bone marrow cells	Active, not recruiting (phase I)
Ex vivo cultured adult allogenic MSCs in ischemic cerebral stroke	Ischemic stroke (10 d); modified Rankin scale ≦4; 20–80 yr; M + F	Intravenous injection of 2 ml/kg allogenic MSCs	Not yet recruiting (phase I/II)
Study of human placenta-derived cells (PDA001) to evaluate the safety and effectiveness for patients with ischemic stroke	Ischemic stroke in MCA or posterior communicating artery territory (no info for recency); NIHSS 6–20; 18–80 yr; M + F	Intravenous injection of 2 lots of 2 or 8 × 10^8/patient, or 1 lot of 2 × 10^6/patient PDA001 cells	Active, not recruiting (phase II)
Study to examine the effects of MultiStem in ischemic stroke	Cortical ischemic stroke (1–2 d); “moderate to moderately severe”; 18–79 yr; M + F	Infusion of MultiStem	Recruiting (phase II)

All information collated from stem cell therapy for stroke trials registered on ClinicalTrials.gov. L, left; R, right; fMRI, functional MRI; M, male; F, female. Inclusion criteria were type of stroke (and days since occurrence of stroke), National Institutes of Health Stroke Score (NIHSS), age of participants, and sex of participants. aConventional therapy: antiplatelet treatment and management in a stroke facility.

References

1. Hu HH. Prevalence of stroke in Taiwan. Stroke. 1989;20(7):858.
2. 邱弘殺. 腦中風之現況與流行病學特徵. 腦中風學會會訊. 2008;15(3).
3. Dirnagl U, Iadecola C, Moskowitz MA. Pathobiology of ischaemic stroke: an integrated view. Trends in Neurosciences. 1999;22(9):391-7.
4. Carmichael ST. Plasticity of Cortical Projections after Stroke. Neuroscientist. 2003;9(1):64-75.
5. Carmichael ST. Cellular and molecular mechanisms of neural repair after stroke: Making waves. Annals of Neurology. 2006;59(5):735-42.
6. Stroemer RP, Kent TA, Hulsebosch CE. Neocortical Neural Sprouting, Synaptogenesis, and Behavioral Recovery After Neocortical Infarction in Rats. Stroke. 1995;26(11):2135-44.
7. Modo M, Stroemer RP, Tang E, Patel S, Hodges H. Effects of Implantation Site of Stem Cell Grafts on Behavioral Recovery From Stroke Damage. Stroke. 2002;33(9):2270-8.
8. Chen J, Li Y, Wang L, et al. Therapeutic Benefit of Intravenous Administration of Bone Marrow Stromal Cells After Cerebral Ischemia in Rats. Stroke. 2001;32(4):1005-11.

9. Chen J, Sanberg PR, Li Y, et al. Intravenous Administration of Human Umbilical Cord Blood Reduces Behavioral Deficits After Stroke in Rats. Stroke. 2001;32(11):2682-8.
10. Chen J, Zhang ZG, Li Y, et al. Intravenous Administration of Human Bone Marrow Stromal Cells Induces Angiogenesis in the Ischemic Boundary Zone After Stroke in Rats. Circ Res. 2003;92(6):692-9.
11. Englund U, Bjrklund A, Wictorin K, Lindvall O, Kokaia M. Grafted neural stem cells develop into functional pyramidal neurons and integrate into host cortical circuitry. Proceedings of the National Academy of Sciences of the United States of America. 2002;99(26):17089-94.
12. Li Y, Chen J, Chen XG, et al. Human marrow stromal cell therapy for stroke in rat: Neurotrophins and functional recovery. Neurology. 2002;59(4):514-23.
13. Li Y, Chen J, Wang L, Lu M, Chopp M. Treatment of stroke in rat with intracarotid administration of marrow stromal cells. Neurology. 2001;56(12):1666-72.
14. Shen LH, Li Y, Chen J, et al. Intracarotid transplantation of bone marrow stromal cells increases axon-myelin remodeling after stroke.

Neuroscience. 2006;137(2):393-9.

15. Shyu W-C, Lin S-Z, Chiang M-F, Su C-Y, Li H. Intracerebral Peripheral Blood Stem Cell (CD34+) Implantation Induces Neuroplasticity by Enhancing beta1 Integrin-Mediated Angiogenesis in Chronic Stroke Rats. J Neurosci. 2006;26(13):3444-53.
16. Zhang ZG, Zhang L, Jiang Q, Chopp M. Bone Marrow-Derived Endothelial Progenitor Cells Participate in Cerebral Neovascularization After Focal Cerebral Ischemia in the Adult Mouse. Circ Res. 2002;90(3):284-8.
17. Bliss T, Guzman R, Daadi M, Steinberg GK. Cell Transplantation Therapy for Stroke. Stroke. 2007;38(2):817-26.
18. Saporta S, Borlongan CV, Sanberg PR. Neural transplantation of human neuroteratocarcinoma (hNT) neurons into ischemic rats. A quantitative dose-response analysis of cell survival and behavioral recovery. Neuroscience. 1999;91(2):519-25.
19. Vendrame M, Gemma C, Mesquita DD, et al. Anti-inflammatory Effects of Human Cord Blood Cells in a Rat Model of Stroke. Stem Cells and Development. 2005;14(5):595-604.
20. Borlongan CV, Hadman M, Davis Sanberg C, Sanberg PR. Central

Nervous System Entry of Peripherally Injected Umbilical Cord Blood Cells Is Not Required for Neuroprotection in Stroke. Stroke. 2004;35(10):2385-9.

21. Kurozumi K, Nakamura K, Tamiya T, et al. Mesenchymal stem cells that produce neurotrophic factors reduce ischemic damage in the rat middle cerebral artery occlusion model. Mol Ther. 2005;11(1):96-104.
22. Llad J, Haenggeli C, Maragakis NJ, Snyder EY, Rothstein JD. Neural stem cells protect against glutamate-induced excitotoxicity and promote survival of injured motor neurons through the secretion of neurotrophic factors. Molecular and Cellular Neuroscience. 2004;27(3):322-31.
23. Jiang Q, Zhang ZG, Ding GL, et al. Investigation of neural progenitor cell induced angiogenesis after embolic stroke in rat using MRI. NeuroImage. 2005;28(3):698-707.
24. Akihiko Taguchi TS, Hidekazu Tanaka, Takayoshi Kanda, Hiroyuki Nishimura, Hiroo Yoshikawa, Yoshitane Tsukamoto, Hiroyuki Iso, Yoshihiro Fujimori, David M. Stern, Hiroaki Naritomi and Tomohiro Matsuyama. Administration of CD34+ cells after stroke enhances neurogenesis via angiogenesisin a mouse model. The journal of clinical

investigation;114(3):330-8.

25. Arvidsson A, Collin T, Kirik D, Kokaia Z, Lindvall O. Neuronal replacement from endogenous precursors in the adult brain after stroke. Nat Med. 2002;8(9):963-70.

26. Jin K, Minami M, Lan JQ, et al. Neurogenesis in dentate subgranular zone and rostral subventricular zone after focal cerebral ischemia in the rat. Proceedings of the National Academy of Sciences of the United States of America. 2001;98(8):4710-5.

27. Smith HK, Gavins FNE. The potential of stem cell therapy for stroke: is PISCES the sign? The FASEB Journal. 2012;26(6):2239-52.

28. Locatelli F, Bersano A, Ballabio E, et al. Stem cell therapy in stroke. Cell Mol Life Sci. 2009;66(5):757-72.

29. Meltzer CC, Kondziolka D, Villemagne VL, et al. Serial [18F] fluorodeoxyglucose positron emission tomography after human neuronal implantation for stroke. Neurosurgery. 2001;49(3):586-91; discussion 91-2.

30. Nelson PT, Kondziolka D, Wechsler L, et al. Clonal Human (hNT) Neuron Grafts for Stroke Therapy: Neuropathology in a Patient 27 Months after Implantation. The American Journal of Pathology. 2002;160(4):1201-6.

Chapter 2
Applicability and Limitations of tracking intracerebral implanted CD 34^{+} stem cells with $R2^{*}$ relaxivity in chronic stroke patients

2.1Backgrounds and purposes

In vivo non-invasive monitoring of the migration and homing of the administered cells is a major concern for stem cell therapy. Magnetic resonance imaging potentially allows for the tracking of the temporal and spatial migration of cells labeled with specific MR contrast agents within brain and tissues.

2.11 How to track the implanted stem cell on MRI: SPIO and gadolinium

MR contrast agents used to label cells can either exhibit properties of being paramagnetic or superparamagnetic (1). These agents alter the T1, T2 and $T2^{*}$ relaxation times of water protons on MRI. Gadolinium chelates with paramagnetism tend to shorten T1 relaxation time more than the T2 and $T2^{*}$ of tissues. SPIO (superparamagnetic iron oxide) nanoparticles with superparamagnetism shorten the T1, T2 and $T2^{*}$ relaxation times of water when present at high concentrations (1).

GRID: Gadolinium-RhodamIne Dextran, which is detectable both in vivo by MRI and subsequently at post-mortem by fluorescent microscopy

(2), is used in animal study only.

SPIO: Superparamagnetic iron oxide. SPIO nanoparticles are being used to efficiently label stem cells for MRI (1, 3-4). Dextran-coated SPIO nanoparticles such as ferumoxides (Feridex, Berlex Laboratories), ferucarbotran (Resovist, Schering Ag) or ferumoxtran (Sinerem, Guerbet) are cationic-coated and designed to attach the negative surface charge of plasma membranes through electrostatic interactions. The SPIO nanoparticles are then incorporated into the endosomes of macrophages (1, 5). Another kind of SPIO nanoparticles such as CliniMACS CD 34 Reagent (Miltenyi Biotech GmbH; Bergisch Gladbach, Germany) is bound to the cell surface via antigen-antibody interaction (6). The CliniMACS system is initially designed to sort $CD34^+$ cells by labeling the CD 34^+ cells with murine monoclonal CD 34 antibody. Unlike the nanoparticles of ferumoxides and Endorem (1, 7), which enter the cell and are present in the cell cytoplasm, the iron-dextran microbeads conjugated to murine monoclonal CD 34 antibody are bound to the cell surfaces of CD 34^+ cells via antigen-antibody interaction (8). It has been proved not to influence the viability, differentiation, and activity of the labeled stem cells (3, 6). It was also proved that the $CD34^+$ cells labeled

with superparamagnetic iron-dextran microbeads, used for specific magnetic sorting, can also be used as a hypointense cell label for in vivo visualization on MRI (6).

2.12 MRI Sequences for quantification of superparamagnetic iron oxide

Stem cells labeled with SPIO contrast agents are usually detected by T2- and $T2^*$-weighted imaging as hypointense foci relative to the normal tissue. Quantifying the number of labeled stem cells in target tissues is of great importance to monitoring the fate of implanted cells. T2-weighted spin echo imaging and multi gradient-echo pulse sequence have been used to quantify the amount of iron within brain (4, 9-10). Rad et al. observed a strong linear correlation between R2 values and labeled cell numbers with different regression lines for different cells types (11). The cluster SPIO labeled cell numbers are also reported to have linear relationship with the $R2^*$ relaxivity (4, 9). Besides, both T2 and $T2^*$ relaxation rates are linearly correlated with cellular iron load and content of freely dissolved iron (4). To achieve high sensitivity for the detection of SPIO nanoparticles, the $T2^*$ relaxation rate is better than the T2 relaxation rate (1, 10).

2.13 Imaging findings in animals

Migration

In vivo tracking of the implanted neural stem cells, the trans-callosal migration of stem cells is proved to be attracted by the lesion site in rats with chronic brain damage following middle cerebral artery occlusion (6, 12-13). In Guzman's study (3), they found stem cell migration with both Prussian blue and the human-specific marker SC 121 staining for their implanted SPIO-labeled human neural stem cells. They also excluded SPIO-laden macrophages with double immunohistochemistry of panmonocytic marker Iba-1 and SC121. When injected in the contra-lateral side of the stroke lesion, the stem cells were observed in the lesions about 10 (6) to 14 (12) days after implantation. A slight degree of migration/relocation of transplanted cells (1-2mm from the injection site) was noted in the cortex and the corpus callosum after 1 to 2 weeks of transplantation into the normal adult mouse brain (14). Similar observations have been reported in another study in which sub-ventricular zone (SVZ) cells injected in a rat striatum migrated 1-1.5mm from the transplantation site 28 days after inoculation (15). Therefore, the migration pattern of the implanted stem cells is influenced by the

implanted and lesion locations.

Phenotypic differentiation of transplanted CD 34^{+} stem cell

One study observed no expression of NeuN (neuronal nuclear antigen, as a neuronal marker) or GFAP (glial fibrilary acidic protein, as an astrocyte marker) one month after CD 34^{+} grafting (6). Goolsby et al. (16) reported that the grafted cells remained CD34^{+} for the first 2 months. The human CD34^{+} expressed neuronal markers such as NeuN and the glial marker GFAP six months after implantation into adult mouse brain.

2.14 The aim of this study

The purpose of this study is to long-term monitor the transplanted stem cells with R2* relaxivity in human subjects. We want to follow up the magnetic resonance characteristics of graft clearance and if there is detectable stem cell migration on 3T MR images.

2.2 Materials and methods

Patients

Institutional review board approval and written informed consent were obtained prior to examination. 15 patients (3 females, 12males; mean age 49.6±9.1years; range 31~65 years) with chronic stroke were prospectively enrolled in this study (during June 2009~July 2011). The inclusion criteria of enrolled patients were: with hemiparetic stroke in the one-sided middle cerebral artery territory, 6-60 months after the onset of stroke, NIHSS scores between 9-20, age between 35-70 years old, no malignant or other major disease.

The stem cells are collected from the patients (autograft). Granulocyte colony –stimulating factor (G-CSF) are injected to amplify the peripheral blood hematopoietic stem cells (PBSCs) of the patients. The mononuclear cells (MNCs) are isolated from peripheral blood using the Ficoll-Histopaque centrifugation method. The $CD34^+$ MNCs were incubated for 30 min at room temperature with 7.5 ml of murine antiCD34 antibody conjugated to iron-dextran microbeads (12 μ g iron per 7.5 ml/vial). The magnetically labeled $CD34^+$ cells were separated from MNCs by a magnetic bead separation method [magnetic-activated

cell sorting (MACS)](Miltenyi Biotec, Gladbach, Germany) (17). Then the patients were sent into the operating room for intracerebral stem cell implantation under MRI-guided navigation. The injected stem cells were 3-8 x 10^6 /250~300 (μL) for each patient. The targets were principally set around the infarction cavity rim (5mm to 10 mm adjacent the rim) from parietal subcortical brain parenchyma to the deeper site along the course of the estimated corticospinal tract

Image acquisition

All MRI studies were performed using a 3.0T GE scanner (GE, Signa, Excite, HDx 3.0 T, Wisconsin, USA) at our center. The serial MRI studies for each patient were scheduled before the stem cell implantation (t1), 1 day (t2), 1 week (t3), 1 month (t4), 3 months (t5), 6 months (t6), and 12 months (t7) after stem cell implantation.

Conventional MRI images

A localizing sagittal T1-weighted images was obtained followed by T2-weighted FSE axial and coronal (4300/100[TR/TE]) images, and T1-weighted FSPGR axial images (5.6/1.8/12). The T1-weighted FSPGR sequence was used for locating the axis for the same patient in different sequences. Diffusion-weighted axial images (b_0=1000) will be obtained

for comparison of the old infarcted lesions and new-onset lesions after operation.

*T2*W multi gradient-echo images*

The iron-dextran beads conjugated to murine monoclonal CD34 antibody (MACS) can be linked to specific antigen on $CD34^+$ cells. The labeled $CD34^+$ cells can be sorted by passing strong magnetic gradients. The superparamagnetic core also makes the labeled cells visible on $T2^*$ weighted gradient-echo images as hypointense signals. Quantitative $R2^*$ relaxivity are performed with a multi-echo gradient-echo sequence with 16 equally spaced echoes; TR=400 msec, first TE/ΔTE= 1.468msec/1.28msec, FOV= 22cm, frequency and phase encoding= 256, slice thickness=5mm, spacing=1mm, flip angle=20°, total scan time=1minute and 46sec.

The implanted graft was detected as hypointense dots with target sign (18) on the T2W gradient image. The residual hypointense dots after one week are usually tiny and faint. Therefore, we chose the 10^{th} echo with TE=13 msec for fuzzy-c means clustering segmentation of the hypointense dots. The $R2^*$ relaxivity of the implanted graft after segmentation is calculated pixel-by-pixel by linear fitting of a

monoexponential decay function ($S(t) = S_0 e^{-t/T2^*}$) to the signal intensities of the 1^{st}~8^{th} echoes (Figure 2.1). We also measured $R2^*$ relaxivity of the contralateral symmetric normal brain parenchyma for comparison. To survey for the possible stem cell migration, the whole brain $R2^*$ map was calculated (Figure 2.2).

Statistical methods

The dependence of mean $R2^*$ values on time was assessed using the two-tailed paired t-test. The significance level was chosen to be 0.05.

Image load

Select the slice with hypointense dot (TE=13msec)

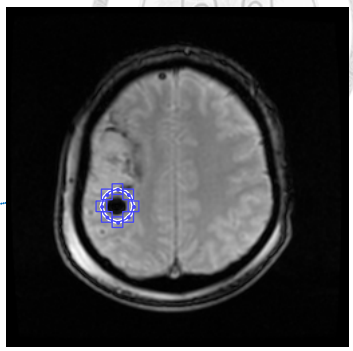

Draw the ROI a little larger than the hypointense area

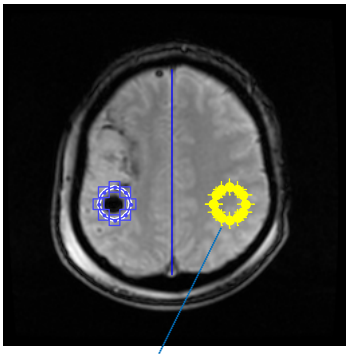

Using "Fuzzy c-means clustering" to perform segmentation

Calculate the $T2^*$ value of each voxel with linear fitting according to equation ($S(t) = S_0 e^{-t/T2^*}$) after segmentation

Calculate $R2^*$ value ($R2^* = 1/T2^*$)

Calculate the mean of $R2^*$ value (all voxels from segmentation)

Calculate the mean of $R2^*$ value of the contralateral ROI?

N

Copy the ROI; paste it in the contralateral symmetric location

Y

Finish to analysis the data at different time points (t1~t7)?

N

Y

Draw the line chart of $R2^*$ with t1~t7 time points

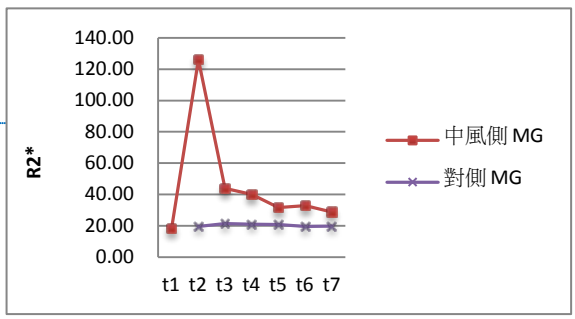

Figure 2.1. Flow chart of longitudinal $R2^*$ measurement for the implanted SPIO-labeled stem cells

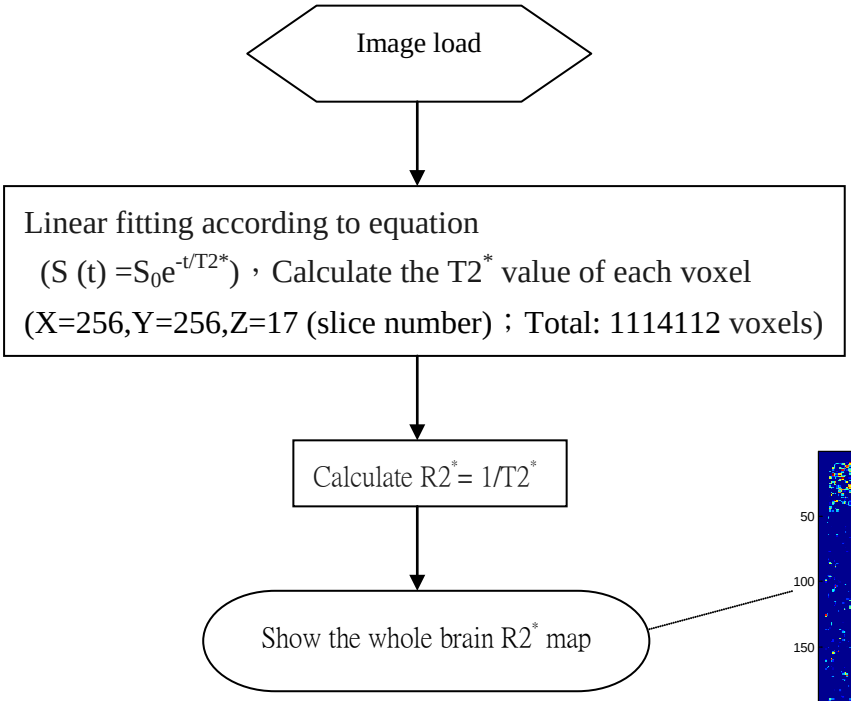

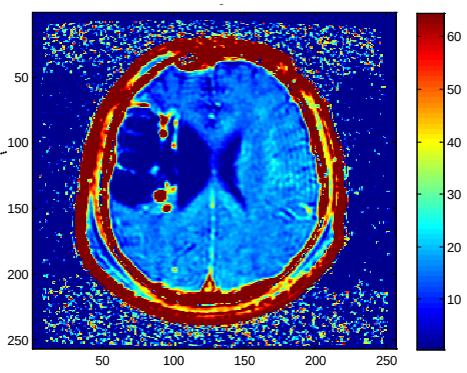

Figure 2.2. Flow chart of whole brain $R2^*$ maps

2.3 Results

The implanted graft can be detected as a target hypointense dot on delayed-echo T2-weighted gradient image (Figure 2.3A) one day after implantation. It also appeared as hypointense dot with mild perifocal edema on T2-weighted FSE image (Figure 2.3B). The procedural-related acute hematoma showed similar hypointensity on both T2W gradient and FSE images (Figure 2.3 C, D). However, the acute hematoma was with irregular shape on T2W gradient image despite the larger volume of hypointensity on FSE image. In the 15 patients received intracerebral implanted grafts, total 36 ROIs of implanted grafts and 8 of acute procedural-related hematomas were detected on T2-weighted gradient and FSE images.

A 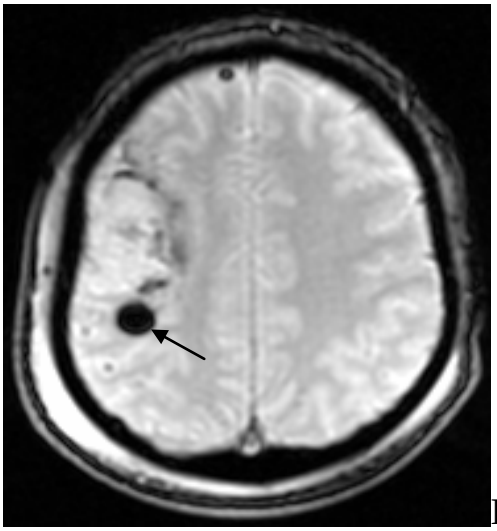 B 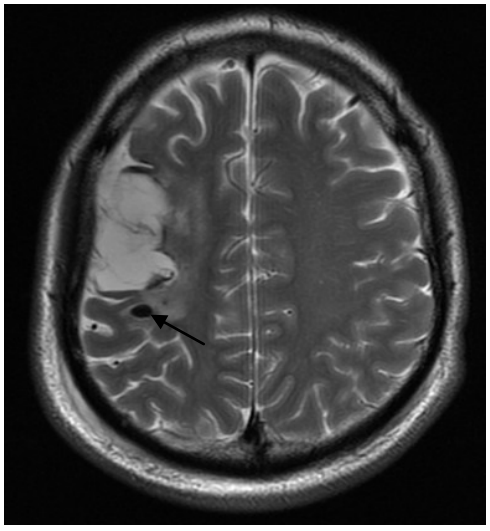

C 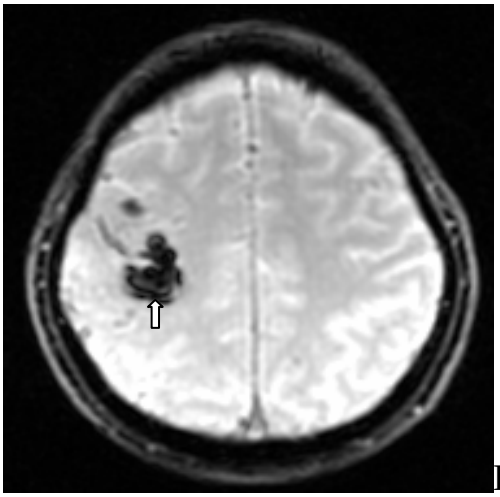 D 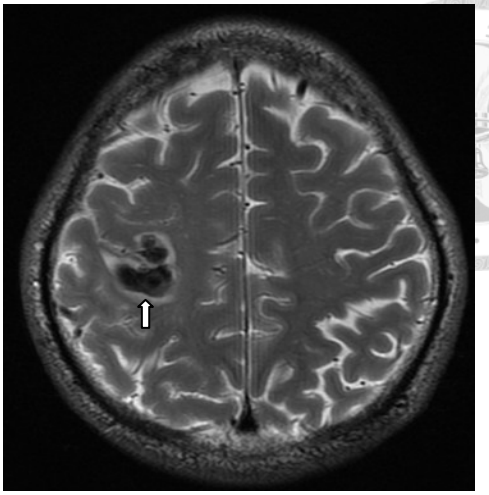

Figure 2.3. The implanted graft and acute procedural-related hematoma on T2W gradient and FSE images. The implanted graft (A, B, black arrow) appeared as a target hypointense dot on T2W gradient image. The acute hematoma was also with hypointensity on T2W gradient and FSE images (C, D, white arrow), but with irregular shape.

2.31 Longitudinal relative quantitative measurement with $R2^*$ values

Total 36 implanted grafts were detected on T2-weighted gradient image. Three implanted grafts were located close to the old hematoma and hard to be separated from the old hematoma. These three ROIs were not included in the longitudinal $R2^*$ relaxivity calculation. The mean $R2^*$ value of the implanted grafts ($134.8\pm37.0\ s^{-1}$) of thirty three ROIs was much higher than that ($18.8\pm2.24\ s^{-1}$) of contralateral symmetric normal brain parenchyma one day (t2) after implantation (Figure 2.4). Four of the 33 ROIs were with complete clearance one week (t3) after implantation

on T2W gradient images. Another two were with complete clearance one month (t4) after implantation. The other 27 ROIs showed persisted residual hypointense dots until the 12-month follow-up (t7). The residual percentage of graft $R2^*$ relaxivity was calculated as [mean $R2^*$(tx)-mean $R2^*$(t1)]/ [mean $R2^*$(t2)-mean $R2^*$(t1)]. The mean $R2^*$ value of implanted graft dropped sharply at t3 (Figure 2.5). The residual mean $R2^*$ relaxivity at t3 was only 26% of that at t2. It further decreased to be 20% at t4 and 19% at t5. The residual mean $R2^*$ relaxivity detected at six-months (t6) and twelve- months (t7) follow-ups were 16% and 12% of the initial values (t2).

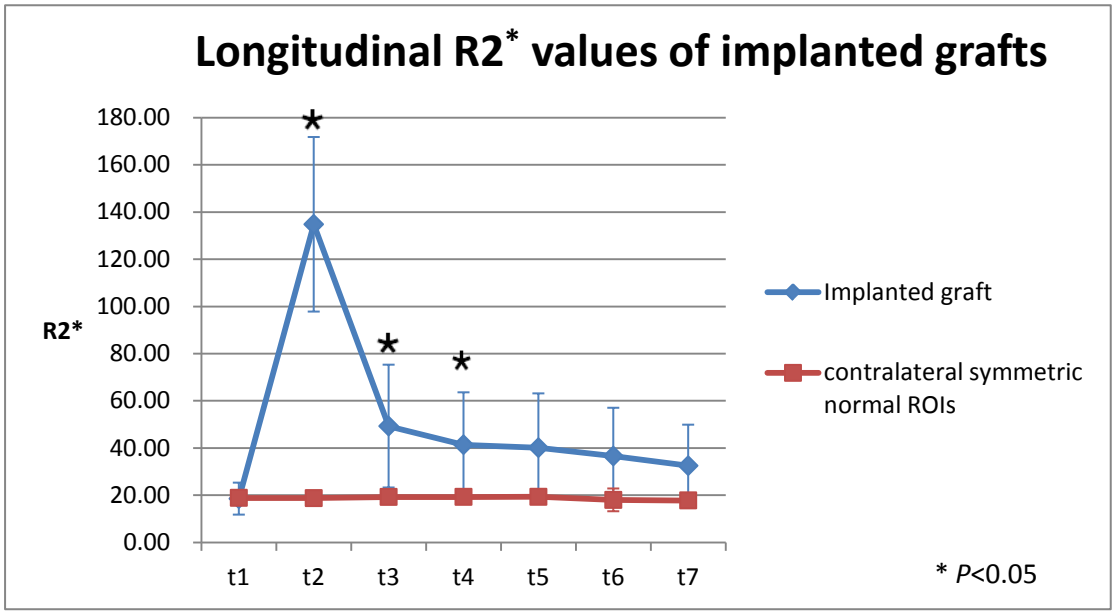

Figure 2.4. Longitudinal $R2^*$ measurement of implanted grafts at the injected sites. Total 33 ROIs in the 15 patients were measured. The mean $R2^*$ values are with significant differences when comparing t2 to t1, t3 to

t2, and t4 to t3 by paired t test.

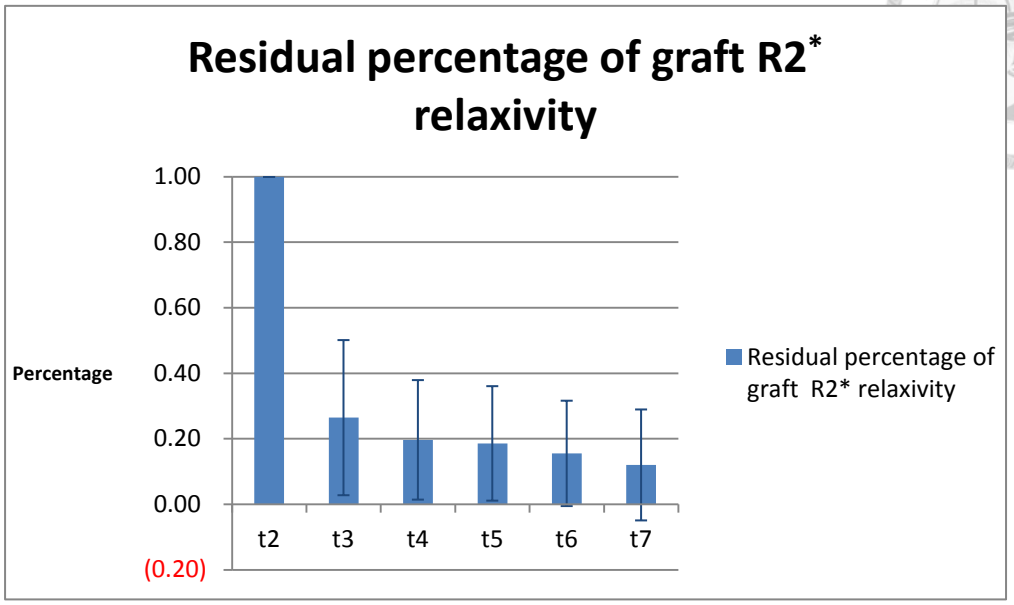

Figure 2.5. The residual percentage of mean graft $R2^*$ relaxivity at the injected sites. The residual percentage was calculated as [mean $R2^*$(tx)-mean $R2^*$(t1)]/ [mean $R2^*$(t2)-mean $R2^*$(t1)]. The residual mean $R2^*$ relaxivity at t3 was only 26% of the one at t2.

Procedural-related macroscopic acute hematomas were detected in eight patients. None of them had new-onset neurologic deficits or signs. The $R2^*$ relaxivity of these eight ROIs were calculated (Figure 2.6). The mean $R2^*$ value of acute hematoma (t2, one day after procedure) is significant higher than the normal brain parenchyma (t1). Note that there is mild increased $R2^*$ value at t5 without statistical significance.

Compared to the longitudinal $R2^*$ line chart of implanted grafts (Figure 2.7), the mean $R2^*$ value of grafts is larger than that of hematoma at t2.

The mean R2* value of grafts decays soon at t3 and afterwards, while the R2* value of hematoma at 12-month follow-up (t7) remains 60.6 % of the R2* value at t2.

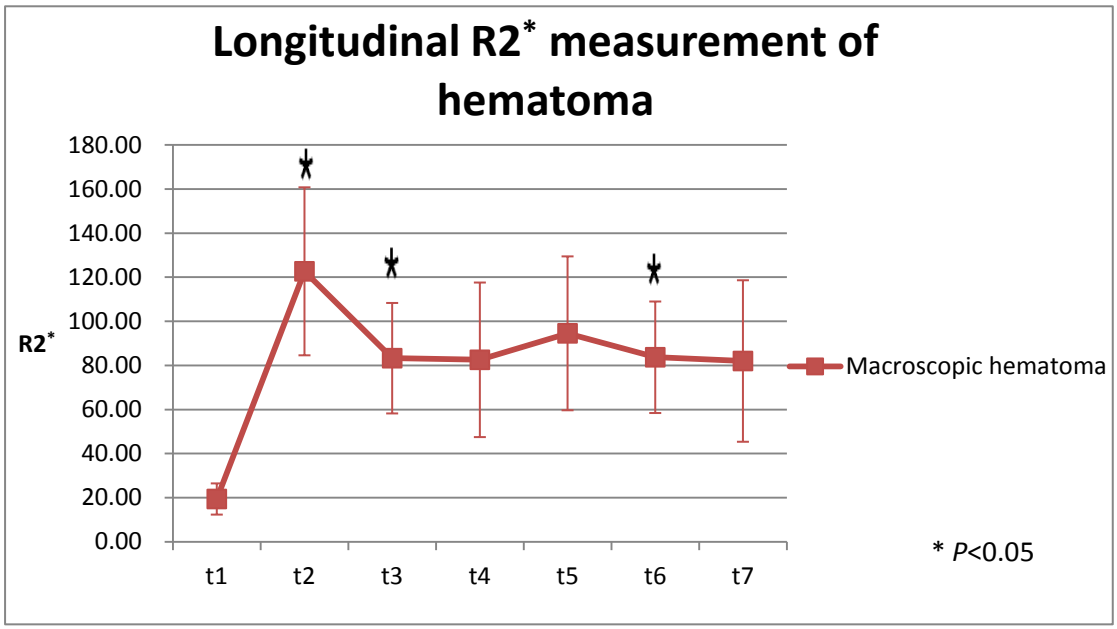

Figure 2.6. The mean R2* relaxivity of procedural-related macroscopic acute hematomas in eight patients. The mean R2* value of acute hematoma (t2, one day after procedure) is significant higher than the normal brain parenchyma (t1). Note that there is mild increased R2* value at t5 without statistical significance.

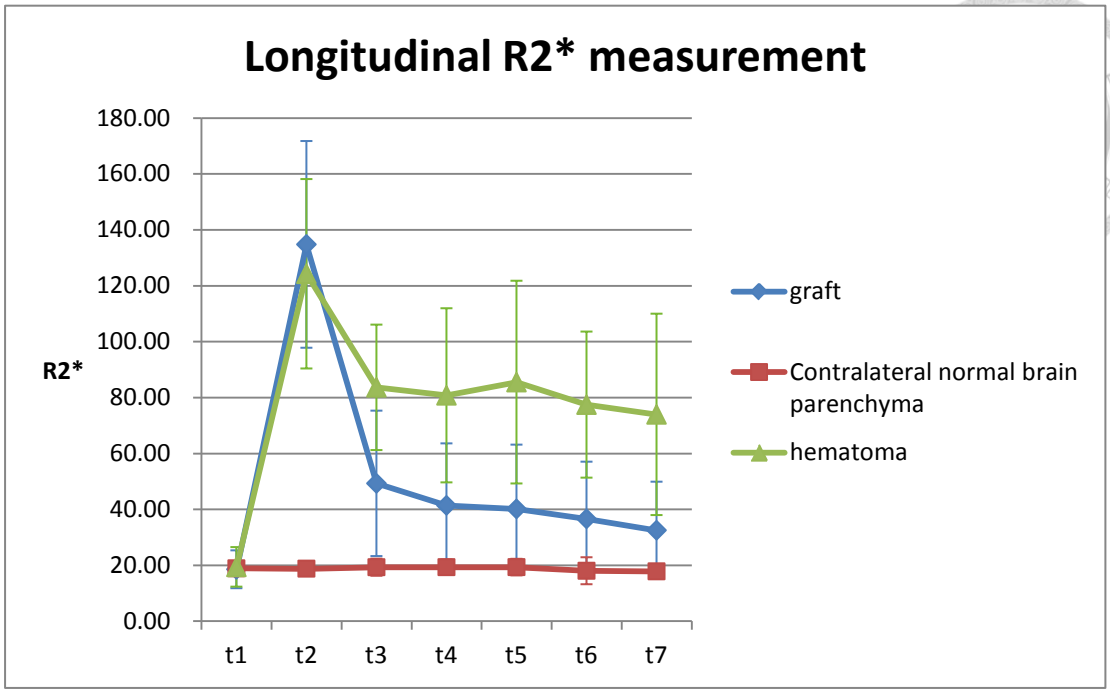

Figure 2.7. Comparisons between the mean $R2^*$ relaxivity of implanted grafts, procedural-related macroscopic acute hematomas, and contralateral symmetric normal brain parenchyma. The mean $R2^*$ value of grafts is larger than that of hematoma at t2. The mean $R2^*$ value of grafts decays soon at t3 and afterwards, while the $R2^*$ value of hematoma at 12-month follow-up (t7) remains 60.6% of the $R2^*$ value at t2.

2.32 Is the persisted residual hypointensity in the injected area SPIO-labeled stem cells?

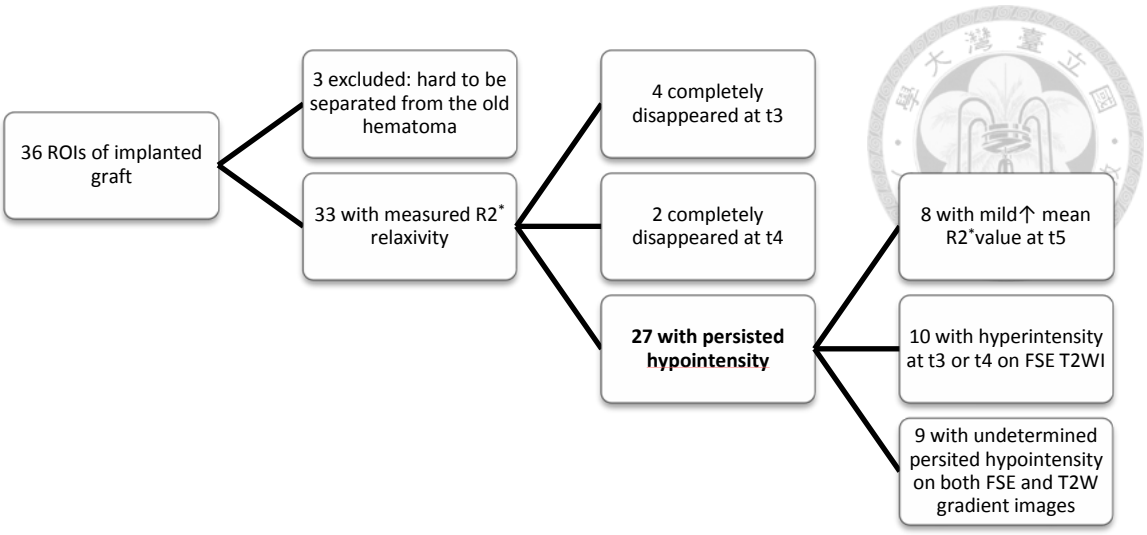

Figure 2.8. Longitudinal monitoring the implanted grafts at the injected sites on T2W gradient and FSE images.

Twenty-seven of the 33 ROIs showed persisted residual hypointense dots until the 12-month follow-up (t7) (Figure 2.8). Two findings raised the possibility of the residual hypointense dots as procedural-related microscopic hemorrhage. Firstly, eight of the 27 ROIs show mild increased $R2^*$ relaxivity at t5 as compared to that of t4 (Figure 2.9) with significant difference by paired t test. This can also proved by increased high $R2^*$ voxel numbers with yellow to red colors at t5 on regional $R2^*$ map (Figure 2.10). Secondly, although the residual dots always showed higher $R2^*$ values than the normal brain parenchyma, ten of the 27 ROIs show central hyperintensity with hypointense rim on FSE T2W images at t3 or t4 (Figure 2.11), which is compatible with the characteristic of

intracranial late subacute hematoma (extra-cellular methemoglobin).

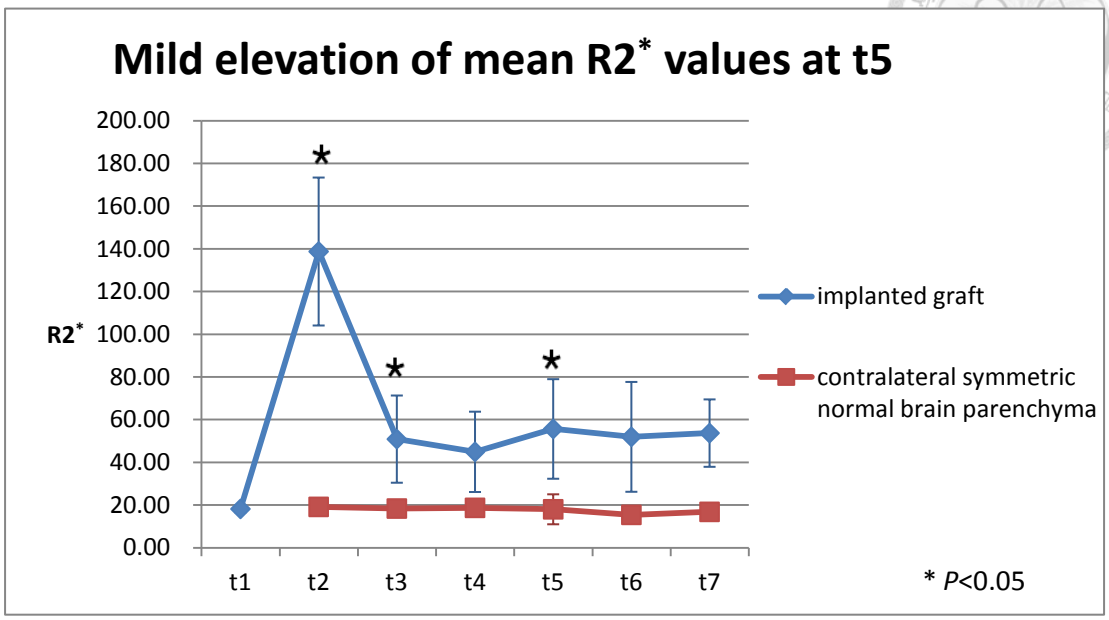

Figure 2.9. The mean R2* relaxivity of eight ROIs with mild increased R2* relaxivity at t5 as compared to that of t4. The mean R2* value at t5 is significant different from that at t4 with *p* value <0.05.

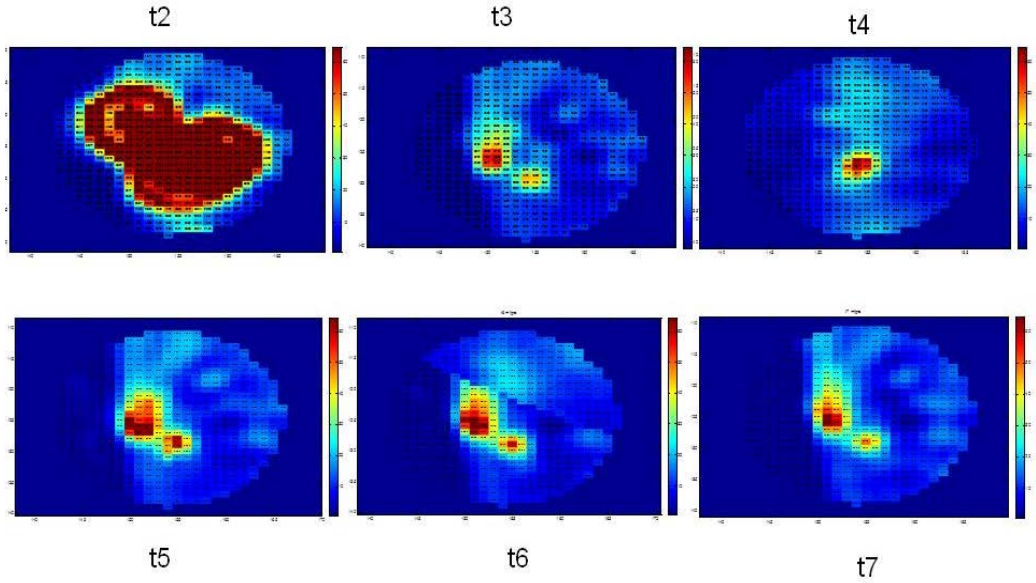

Figure 2.10. The regional R2* map at the implanted site. Note that there are increased voxel numbers with higher R2* values (yellow to red colors) at t5 as compared to t4.

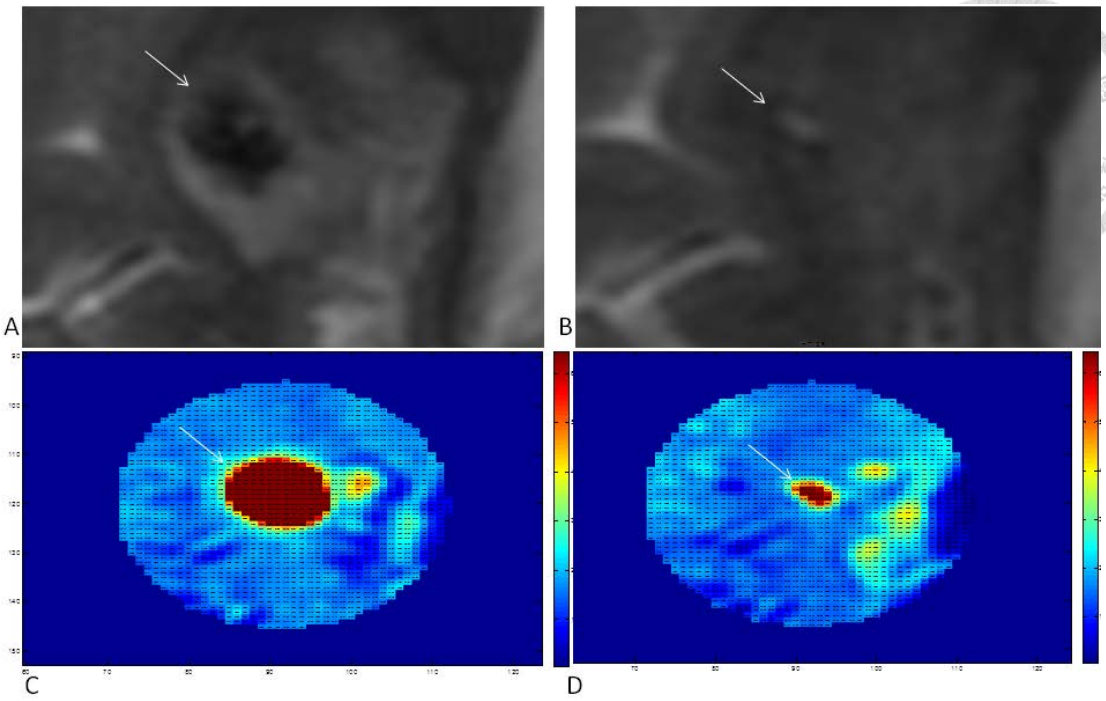

Figure 2.11. Procedural-related hematoma mixed in the implanted graft. The implanted graft was with hypointensity on T2W FSE image (A, white arrow) and ovoid nodule with high $R2^*$ values on regional $R2^*$ map (C, white arrow). The residual high $R2^*$ nodule on the one-month follow-up $R2^*$ map (D, white arrow) was with central hyperintensity and hypointense rim on T2W FSE image (B, white arrow).

2.33 Is there any migration?

Only one of the 36 implanted grafts showed possible regional migration along the infarcted lesion. The migration was more prominent on 3-month and 6-month follow-up $R2^*$ maps. The migrated distance was about 5mm and similar at t6 and t7 which make the possibility of slice position change between different scan times less likely (Figure 2.12).

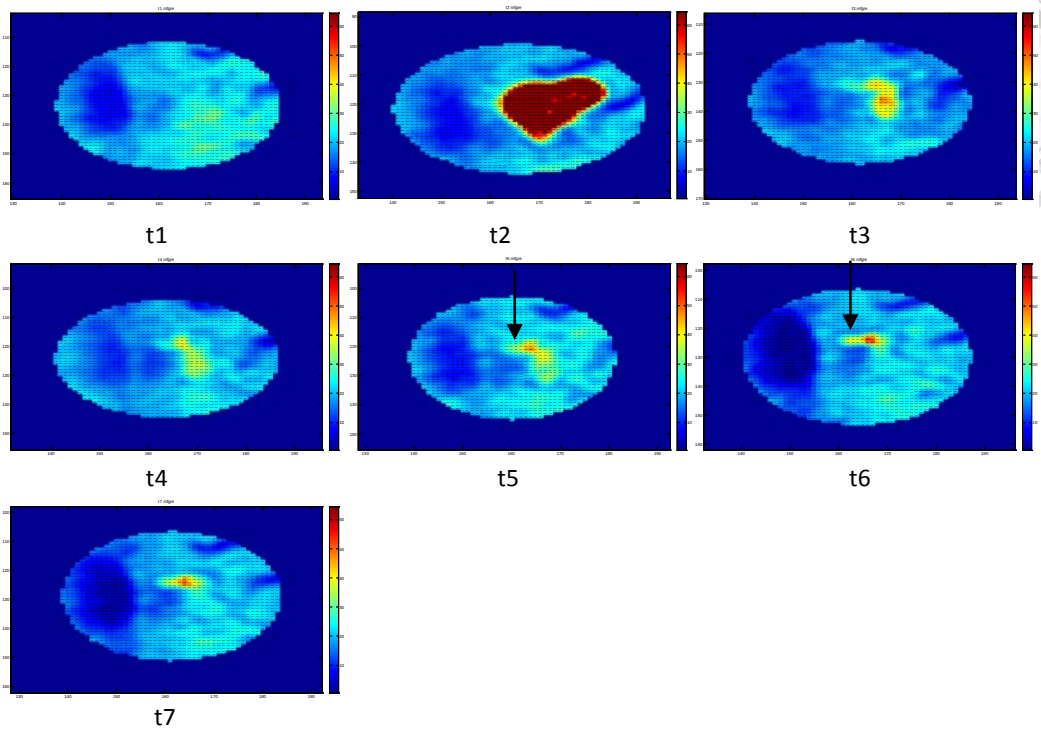

Figure 2.12.Regions R2* map of one implanted graft with possible migration. The higher-R2* voxles migrate along the infarcted lesion (black arrow). The migration was more prominent on 3-month (t5) and 6-month (t6) follow-up R2* maps. The migrated distance was about 5mm and similar at t6 and t7 which make the possibility of slice position change between different scan times less likely.

Procedural-related hemorrhage mimicking SPIO-labeled stem cell migration

Two patients with procedural-related hemorrhage adjacent to the implanted grafts were initially mistaken as stem cell migration in the follow-up gradient images. These two patients both had old hemorrhagic

cavities in the right basal ganglia (Figure 2.13A, 2.14A). One of the implanted grafts was located in the anterior aspect of the cavity (Figure 2.13B, F) and the other was about 5mm lateral to the cavity (Figure 2.14B, D). The signal of acute hematoma was presumed to be hypointensity on FSE T2WI. When mixing with strong hyperintensity of CSF, it may become intermediate signal on FSE T2WI. The intermediate signal of the acute hematoma makes it easy to be missed on image interpretation. (Figure 2.13B, 2.14B). Tiny residual graft in the anterior aspect of the cavity and hemosiderine deposition around the posterior aspect of the cavity were shown on one-week follow up FSE T2W image (Figure 2.13C) and $R2^*$ map (Figure 2.13G). The hemosiderine deposition may be mistaken as graft migration if one misses to detect the acute hematoma. Besides, the hematoma may fill the cavity in the later follow-up image (Figure 2.14F), which also mimics graft migration. The cavities were shrinkage with possible hemosiderine deposition around the posterior aspect and lateral intermediate band formation, which is possible gliosis formation. The appearance represents repeat bleeding with remodeling process of the previous hemorrhagic cavity in the 12-month follow-up.

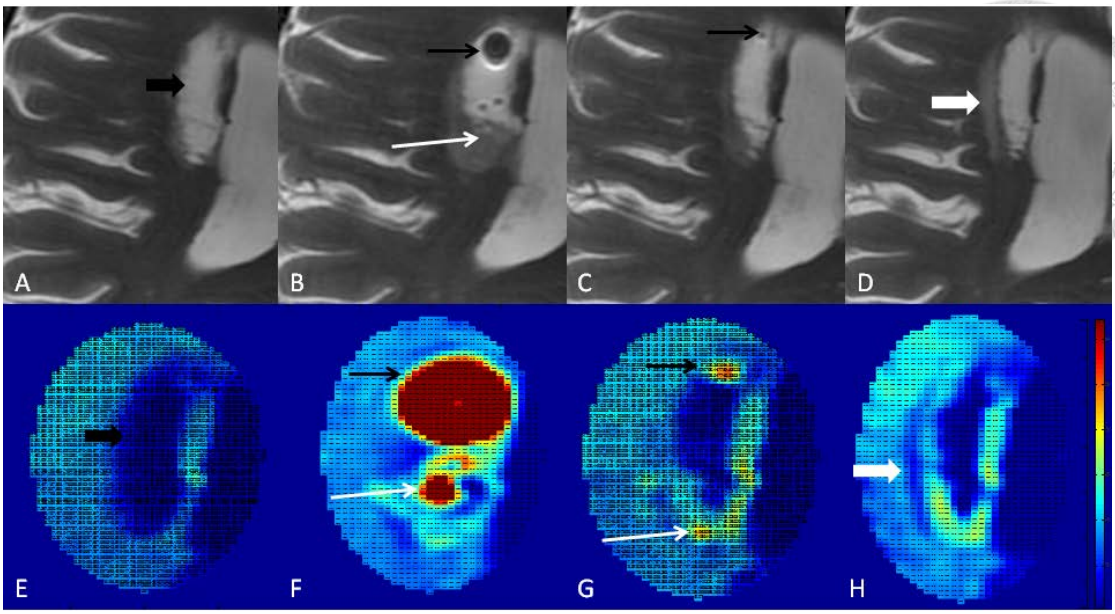

Figure 2.13. Procedural-related bleeding mimicking migration of the implanted graft (1). A, E) Old hemorrhagic cavity (black arrow) was in the right basal ganglion. B, F) One day follow-up, the implanted graft (black arrow) was located in the anterior aspect of the cavity. Procedural-related acute hematoma (white arrow) was in the dependent side of the cavity. The signal of acute hematoma was presumed to be hypointensity on FSE T2WI. It was mixed with strong hyperintensity of CSF and became intermediate signal on FSE T2WI. The intermediate signal of the acute hematoma makes it easy to be missed on image interpretation. C, G) One week follow-up, hemosiderine deposition (white arrow) around the posterior aspect of the cavity mimics graft migration. Tiny residual graft was located in the anterior aspect of the cavity (black arrow). D, H) the cavity is shrinkage with possible

hemosiderine deposition around the posterior aspect and lateral intermediate band formation (white arrow), which is possible gliosis formation. The appearance represents repeat bleeding with remodeling process of the hemorrhagic cavity in the 12-month follow-up.

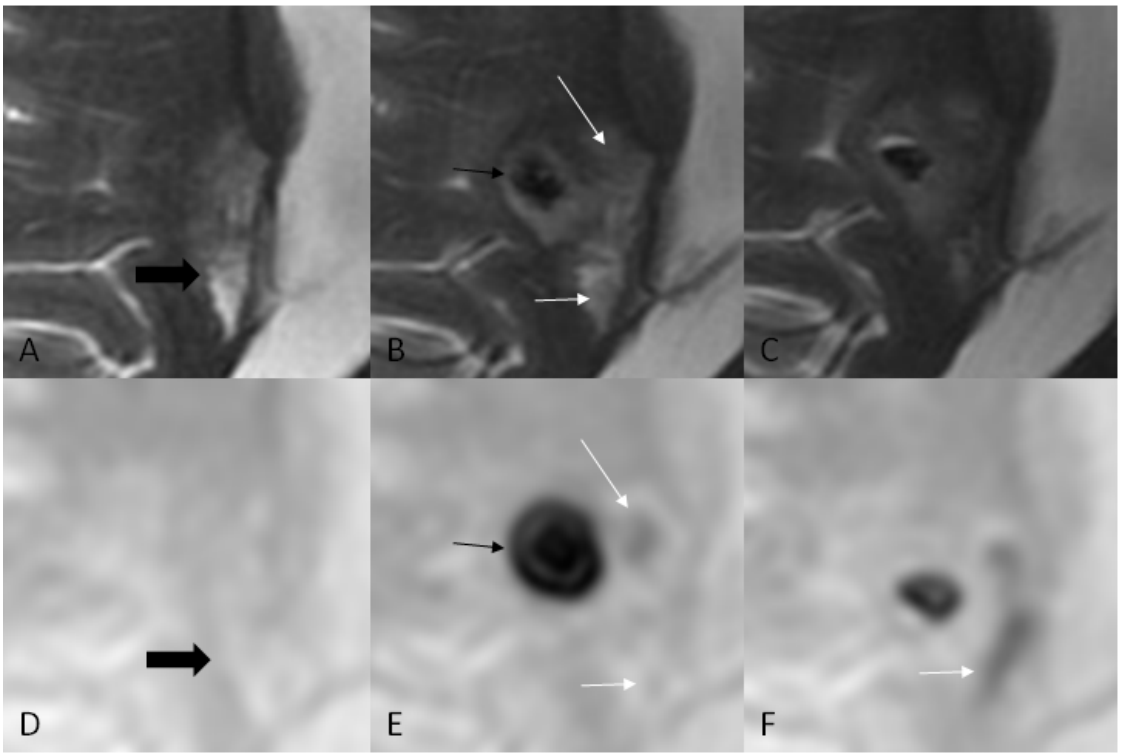

Figure 2.14. Procedural-related bleeding mimicking migration of the implanted graft (2). A, D) Old hemorrhagic cavity (black arrow) was in the right basal ganglion. B, E) One day follow-up, the implanted graft (black arrow) was located laterally to the cavity. Procedural-related acute hematoma (white arrow) was in the anterior and posterior aspects of the cavity. C, F) the hematoma filled the cavity with hypointensity on T2W gradient image (white arrow) which mimics migration of the implanted

graft.

Artifacts by veins, physiologic calcification and previous old hematoma

The veins with deoxygenated blood have the paramagnetic characteristics and show higher $R2^*$ values compared to the normal brain parenchyma on the whole brain $R2^*$ map (Figure 2.15A). The higher $R2^*$ voxels in the corpus callosum and basal ganglia resulting from veins can mimic SPIO-labeled stem cell migration. Besides, Iron deposition in the bilateral basal ganglia and hemosiderine deposition from previous hemorrhage may also interfere with the tracking of SPIO-labeled stem cell on $R2^*$ map (Figure 2.15B).

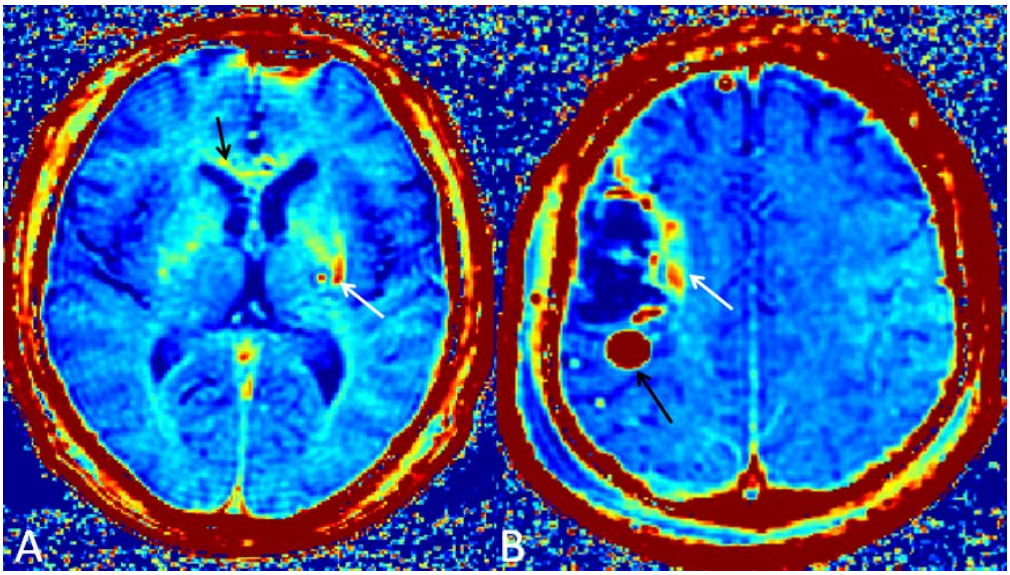

Figure 2.15. Artifacts on whole brain $R2^*$ map. A) The higher $R2^*$ voxels in the corpus callosum (black arrow) and basal ganglion (white arrow)

resulting from veins can mimic SPIO-labeled stem cell migration on follow-up images. B) hemosiderine deposition from previous hemorrhage also interfere with the tracking of SPIO-labeled stem cell on $R2^*$ map.

2.4Discussion

Longitudinal R2 value of grafts and hematoma*

Peripheral blood stem cells (PBSC) (CD 34^+) are reported to promote functional recovery in the animal stroke models (19-21). With regular MRI follow-ups of chronic stroke patients in one phase II clinical trial, $R2^*$ relaxivity was applied to tracking the intracerebral implanted PBSC. Based on the hypothesis of linear relationship between the $R2^*$ relaxivity and SPIO labeled cell numbers (4, 9, 11), we measured the local longitudinal $R2^*$ relaxivity in the injected site to monitor the clearance pattern of the implanted stem cells.

The implanted graft appear as target hypodense dots which is the result of the combination of a point magnetic dipolar field and consequent intravoxel dephasing patterns in the section-select direction on T2W gradient image (18). The $R2^*$ value measured one day after implantation is remarkable higher than that of the contralateral symmetric brain tissue. However, the $R2^*$ value drops sharply at one-week follow-up with only 26% residual of initial values. It further decreased to be 20% at one-month follow up. Three findings in the animal studies may explain for the early clearance of the majority implanted grafts. First, this

imaging finding was similar to Walczak's study (22) which had a surprisingly sharp cutoff rather than a gradual decrease of signal at 6 days post-grafting. It is proved that significant cell replication occur post-transplantation, causing rapid dilution of Feridex particles between mother and daughter cells toward undetectable levels. Second, cell death may also result in partial early signal loss. Guzman et al (3) showed early volume loss of dead implanted graft at days 7 and 35 post implantation, whereas viable graft remained unchanged. Third, animal studies have shown migration of contra-lateral implanted stem cells from the injection sites to be re-populated in the peri-lesional areas 10~14 days after implantation (7, 12, 23). Therefore, the most important timing for the fate of majority implanted graft is in the first week after implantation. The implanted grafts may survive with replication and migration or die with macrophage clearance.

27 of 33 implanted graft ROIs show persisted residual T2W gradient hypointensity one month after implantation and last until the end (12 month) of follow-up in this study. Is the persisted residual hypointensity representing stem cell, microhemorrhage, or iron-loaded macrophages? Two findings in our study indicate that the persisted hypointensity may

be the procedural-related microhemorrhage. Fist, the residual hypointense graft ROIs on T2W gradient images became hyperintense at one week or one month follow-up on FSE T2W images which may be the subacute hematoma with methemoglobin contents (24). Second, eight of the 27 ROIs show mild increased $R2^*$ relaxivity at 3-month follow-up as compared to that of one-month follow-up. This finding is also shown on our longitudinal $R2^*$ line chart of procedural-related macroscopic intracranial hematoma. This may be resulted from the blood products evolution of methemoglobin to become hemosiderine in the 3-month follow up. The hemosiderin have about ten thousand unpaired electrons with superparamagnetic characteristic (24) which result in higher $R2^*$ relaxivity than that of paramagnetic methemoglobin in the subacute stage. However, 9 of the 27ROIs with residual persisted hypointensity did not show image evidence of microhemorrhage. In Terrovitis's study (25), large intramyocardial MR signal voids persisted at 3 weeks (50%~90% of initial signal). Histology revealed the presence of iron-containing macrophages at the injection site, but very few stem cells in the animals transplanted with syngeneic cells. Iron-loaded macrophages may be explained for the undetermined residual persisted hypointensity on

12-months follow-up T2W gradient images.

Possible migration

Long distance migration of contra-lateral implanted stem cells from the injection sites to be re-populated in the peri-lesional areas has been shown in the animal studies (7, 12, 23). The proposed hypothesis is that the long distance transcallosal migration observed in the stroke-lesioned animals is due to neural stem cells being attracted by the lesion site (12). If transplantation was adjacent to the lesion, no targeted migration was found with more than 1mm distance between the lesion and the graft site in the rat brain (3). The implanted grafts in our study were planned to be implanted 5~10mm adjacent to the infarcted rim. Our implanted locations were not within 1mm to the old infarcted lesions. Only one implanted-graft ROI showed possible migration on $R2^*$ map (Figure 2.12). The migration was more prominent shown on 3-month to 6-month follow-ups. The migration timing was much later than that of stem cells in animal studies (10~14 days after implantation). Besides of SPIO-labeled cell migration, iron-loaded macrophages migration should also be taken into consideration for this image finding.

Two patients have old hemorrhagic cavities with procedural-related

hematomas which were initially mistaken as SPIO-labeled stem cell migration. The acute hematoma on 1-day follow up FSE T2W image is with intermediate signal intensity in the cavity which was filled with fluid before implantation. When the hypointense (deoxyhemoglobin) acute hematoma was mixed with the hyperintense cerebrospinal fluid, it showed as intermediate signal on FSE T2W image. The intermediate signal of acute hematoma makes it easy to be missed on imaging interpretation. Then the hematoma became methemoglobin and pooled in the dependent-side of the cavity on 1-week follow up T2W gradient images. It mimics stem cells migration in the cavity in Zhu's study (26).

Complication

Though 8 patients have small procedural-related macroscopic hemorrhage detected immediately on one-day follow-up MRI, none of them developed new neurologic deficits and signs.

Limitations of detection of SPIO at 3.0T using $R2^*$ relaxivity

Resolution

In this preliminary clinical trial, we applied $R2^*$ relaxivity to track the implanted SPIO-labeled stem cells. The lower detection limits are influenced by different stem cells (11), method of labeling (6), voxel

size, field strength, and parameters of the protocols. For comparison the result of $R2^*$ values to different sequences (FSE T2WI and MR perfusion) in our study, the slice thickness was set with 5 mm in all sequences. Though the larger voxel size increases the signal-noise ratio, the detection limit of stem cells also increases (27). With similar voxel size (256 x 256, slice thickness:5mm), the detection limit in brain tissue is approximlately 600cells/voxel with Resovist labeling in Dahnke's study (27). If the residual SPIO-labeled stem cells disperse under duplication and/or migration, the cell numbers in the region of interest may be under the detection limit in the region of interest. Then using the $R2^*$ values to track stem cells may underestimate the residual stem cells.

Macroscopic susceptibilities

The $R2^*$ relaxivity is not only influenced by SPIO labeled on stem cells, but also by macroscopic susceptibilities that arise from air-brain interface, deoxyhemoglobin in cortical veins, irons in the bilateral basal ganglia, and hemosiderine deposition from previous hemorrhage. These disturbances cause enhanced signal decay. Therefore, susceptibility artifacts lead to obscure small concentrations of SPIO-labeled cells and make the migration with small cell numbers undetectable.

2.5 Conclusion

The $R2^*$ values of implanted grafts drops sharply in one month with only 20% residual of the values at one-day follow-up. It may indicate that the most important timing for the fate of implanted stem cells (migration/homing, survival/proliferation, and death/clearance) is within one month after implantation. Despite the early clearance/dispersion of the majority grafts, persisted residual hypointense dots until the end of the study (12-month follow up) are common at the injected sites (27/33, 81.8%). Two thirds of the persisted residual T2W gradient hypointense dots may be related to procedural-related microhemorrhage with image evidences.

2.6 Publication

Conference paper

1. (2011) **Chao-Chun Lin**, Wu-Chung Shen, Yu- Chien Lo, Yung-Jen Ho, Hsiao-Wei Peng, Chia-Wei Lin, Hing-Chiu Chang, Jui-Fen Chen, Hsiao-Wen Chung, Woei-Cherng Shyu, Shinn-Zong Lin. **Longitudinal tracking of intracerebral implanted stem cells by $R2^*$ relaxivity in chronic stroke patients.** *ASNR 49th Annual Meeting & the Foundation of the ASNR Symposium 2011*, Seattle, USA (Oral presentation 408)

References

1. Arbab AS, Liu W, Frank JA. Cellular magnetic resonance imaging: current status and future prospects. Expert Rev Med Devices. 2006;3(4):427-39.
2. Modo M, Cash D, Mellodew K, et al. Tracking tansplanted stem cell migration using bifunctional, contrast agent-enhanced, magnetic resonance imaging. NeuroImage. 2002;17(2):803-11.
3. Guzman R, Uchida N, Bliss TM, et al. Long-term monitoring of transplanted human neural stem cells in developmental and pathological contexts with MRI. Proceedings of the National Academy of Sciences. 2007;104(24):10211-6.
4. Kuhlpeter R, Dahnke H, Matuszewski L, et al. R2 and R2* mapping for sensing cell-bound superparamagnetic nanoparticles: in vitro and murine in vivo testing. Radiology. 2007;245(2):449-57.
5. Fleige G, F S, D L. In vitro characterization f two different ultrasmall iron oxide particles for magnetic resonance cell tracking. Invest Radiol. 2002;37(9):482-8.
6. Jendelová PH, Vít; Urdziková, Lucia; Glogarová, Kateřina; Rahmatová, Šárka; Fales, Ivan; Andersson, Benita; Procházka, Pavel; Zamečník,

Josef; Eckschlager, Tomáš; Kobylka, Petr; Hájek, Milan; Syková, Eva. Magnetic Resonance Tracking of Human CD34 Progenitor Cells Separated by Means of Immunomagnetic Selection and Transplanted Into Injured Rat Brain. Cell Transplantation. 2005;14:173-82.

7. Jendelová P, Herynek V, Urdzíková L, et al. Magnetic resonance tracking of transplanted bone marrow and embryonic stem cells labeled by iron oxide nanoparticles in rat brain and spinal cord. Journal of Neuroscience Research. 2004;76(2):232-43.
8. Richel DJ. Highly purified CD34+ cells isolated using magnetically activated cell selection provide rapid engraftment following high-dose chemotherapy in breast cancer patients. Bone marrow transplantation. 2000;25(3):243.
9. Liu W, Dahnke H, Rahmer J, Jordan EK, Frank JA. Ultrashort T2* relaxometry for quantitation of highly concentrated superparamagnetic iron oxide (SPIO) nanoparticle labeled cells. Magn Reson Med. 2009;61(4):761-6.
10. Langkammer C, Krebs N, Goessler W, et al. Quantitative MR imaging of Brain Iron: A Postmortem Validation Study. Radiology. 2010;257(2):455-62.

11. Rad AM, Arbab AS, Iskander ASM, Jiang Q, Soltanian-Zadeh H. Quantification of superparamagnetic iron oxide (SPIO)-labeled cells using MRI. Journal of Magnetic Resonance Imaging. 2007;26(2):366-74.
12. Modo M, Mellodew K, Cash D, et al. Mapping transplanted stem cell migration after a stroke: a serial, in vivo magnetic resonance imaging study. Neuroimage. 2004;21(1):311-7.
13. Kim D-E, Schellingerhout D, Ishii K, Shah K, Weissleder R. Imaging of Stem Cell Recruitment to Ischemic Infarcts in a Murine Model. Stroke. 2004;35(4):952-7.
14. Magnitsky S, Watson DJ, Walton RM, et al. In vivo and ex vivo MRI detection of localizaed and disseminated neural sem cell grafts in the mouse brain. NeuroImage. 2005;26:744-54.
15. Zhang RL, Zhang L, Zhang ZG, et al. Migration and differentiation of adult rat subventricular zone progenitor cells transplanted into the adult rat striatum. Neuroscience. 2003;116:373-82.
16. Goolsby J, Marty MC, Heletz D, et al. Hematopoietic progenitors express neural genes. Proceedings of the National Academy of Sciences of the United States of America. 2003;100(25):14926-31.

17. Handgretinger R, Lang P, Ihm K, et al. Isolation and transplantation of highly purified autologous peripheral CD34(+) progenitor cells: purging efficacy, hematopoietic reconstitution and long-term outcome in children with high-risk neuroblastoma. Bone marrow transplantation. 2002;29(9):731-6.
18. Kim JK, Kucharczyk W, Henkelman RM. Cavernous hemangiomas: dipolar susceptibility artifacts at MR imaging. Radiology. 1993;187(3):735-41.
19. Akihiko Taguchi TS, Hidekazu Tanaka, Takayoshi Kanda, Hiroyuki Nishimura, Hiroo Yoshikawa, Yoshitane Tsukamoto, Hiroyuki Iso, Yoshihiro Fujimori, David M. Stern, Hiroaki Naritomi and Tomohiro Matsuyama. Administration of CD34+ cells after stroke enhances neurogenesis via angiogenesisin a mouse model. The Journal of Clinical Investigation;114(3):330-8.
20. Shen LH, Li Y, Chen J, et al. Intracarotid transplantation of bone marrow stromal cells increases axon-myelin remodeling after stroke. Neuroscience. 2006;137(2):393-9.
21. Shyu W-C, Lin S-Z, Chiang M-F, Su C-Y, Li H. Intracerebral Peripheral Blood Stem Cell (CD34+) Implantation Induces

Neuroplasticity by Enhancing beta1 Integrin-Mediated Angiogenesis in Chronic Stroke Rats. J Neurosci. 2006;26(13):3444-53.

22. Walczak P, Kedziorek DA, Gilad AA, Barnett BP, Bulte JWM. Applicability and limitations of MR tracking of neural stem cells with asymmetric cell division and rapid turnover: The case of the Shiverer dysmyelinated mouse brain. Magnetic Resonance in Medicine. 2007;58(2):261-9.

23. Hoehn M, Küstermann E, Blunk J, et al. Monitoring of implanted stem cell migration in vivo: A highly resolved in vivo magnetic resonance imaging investigation of experimental stroke in rat. Proceedings of the National Academy of Sciences. 2002;99(25):16267-72.

24. Gomori JM, Grossman RI. Mechanisms responsible for the MR appearance and evolution of intracranial hemorrhage. Radiographics. 1988;8(3):427-40.

25. Terrovitis J. Magnetic resonance imaging overestimates ferumoxide-labeled stem cell survival after transplantation in the heart. Circulation. 2008;117(12):1555.

26. Zhu J, Zhou L, XingWu F. Tracking Neural Stem Cells in Patients

with Brain Trauma. New England Journal of Medicine. 2006;355(22):2376-8.

27. Dahnke H, T S. Limits of Detection of SPIO at 3.0 T Using T2* Relaxometry. Magnetic Resonance in Medicine. 2005;53:1202-6.

Chapter 3

3.1 Backgrounds and purposes

A growing number of studies in animal model highlight the potential of stem cell transplantation as a novel therapeutic approach for stroke. Despite unclear underlying mechanisms of transplanted cell-mediated recovery, improvement of various stroke-induced behavioral deficits has been observed in many animal studies (1-8)

Taguchi et al. (9) have demonstrated that systemic administration of human cord blood-derived CD 34^+ cells to immunocompromised mice subjected to stroke 48 hours earlier induces neovascularization in the ischemic zone and provides a favorable environment for neuronal regeneration. Another study (8) also found that intracerebral peripheral blood stem cell (PBSC) ($CD34^+$) implantation induces neuroplasticity by angiogenesis in chronic stroke rats. Their results showed a significant increase in relative cerebral blood flow (rCBF) in the middle cerebral artery cortex of the ischemic brain in the PBSC-treated rats compared with control rats. Besides, the angiogenesis occurred before the cortical plasticity in the animal studies. If this is also true in human subjects, the rCBV and rCVF will increase substantially before the clinical

neurological function improvement. In this study, we want to test the hypothesis of increased cerebral blood flow and volume associated with $CD34^+$ stem cell implantation by MR $T2^*$ perfusion sequence. To our knowledge, this is the first study to investigate the longitudinal perfusion change after intracerebral stem cell implantation in chronic stoke patients.

3.2 Materials and methods

Patients

15 patients (3 females, 12males; mean age 49.6±9.1years; range 31~65 years) with chronic stroke were prospectively enrolled in this study (during June 2009~July 2011). The inclusion criteria of enrolled patients were: with hemiparetic stroke in the one-sided middle cerebral artery territory, 6-60 months after the onset of stroke, NIHSS scores between 9-20, age between 35-70 years old, no malignant or other major disease.

The stem cells are collected from the patients (autograft). Granulocyte colony –stimulating factor (G-CSF) are injected to amplify the peripheral blood hematopoietic stem cells (PBSCs) of the patients. The mononuclear cells (MNCs) are isolated from peripheral blood using the Ficoll-Histopaque centrifugation method. The $CD34^+$ MNCs were separated from MNCs by a magnetic bead separation method [magnetic-activated cell sorting (MACS)](Miltenyi Biotec, Gladbach, Germany). Then the patients were sent into the operating room for intracerebral stem cell implantation under MRI-guided navigation. The injected stem cells were about 3-8 x 10^6 /250~300 (μL) for each patient. The targets were principally set around the infarction cavity rim

(5mm to 10 mm adjacent the rim) from parietal subcortical brain parenchyma to the deeper site along the course of the estimated corticospinal tract

Image acquisition

All MRI studies will be performed using a 3.0T GE scanner (GE, Signa, Excite, HDx 3.0 T, Wisconsin, USA) at our center. The serial MR perfusion studies for each patient were scheduled before the stem cell implantation (T1), 1 day (T2), 1 week (T3), 1 month (T4), 3 months (T5), 6 months (T6), and 12 months (T7) after stem cell implantation. A localizing sagittal T1-weighted images was obtained followed by T2-weighted axial (4300/100[TR/TE]) images.

Dynamic contrast agent-enhanced $T2^*$-weighted gradient-echo echo-planar images (1500/50/90[TR/TE/Flip angle], total scan time=1min30sec) were acquired during the first pass of a full dose (19cc/patient) bolus of gadopentetate dimeglumine (Magnevist; Berlex Laboratories, Wayne, NJ). The injection rate is 4cc/sec, followed by normal saline 20cc, 4cc/sec. 13 sections were selected for perfusion MR imaging through the old infracted lesion based on FSE (fast spine echo)

T2-weighted images.

Data Processing for Perfusion

Data processing was performed by using nICE (Nordic ICE, Nordic Imaging Lab, Norway) software.

The AIF (arterial input function) deconvolution is not applied in our study. Hence both CBV and CBF are only determined in a relative sense based on the properties of the first-pass tissue response curve. From this curve, relative CBV is estimated from the area under the first-pass curve (AUC). The relative CBF and mean transit time, which can be derived using different means, are estimated in our study using the following method for better immunity to delay and dispersion effects (10):

MTT from first moment: With this approach, MTT is estimated from the normalized first moment of the first-pass curve: rMTT = fmAUC/AUC and rCBF=AUC/rMTT where fmAUC is the first moment of the area under the first-pass curve.

We measure the region of interest (ROI) around the stem cell implanted foci. One well-trained technologist (C.Y.W. with three-year MR experience) draws the ROIs. The measurements were performed by C.Y.W twice with mean values to reduce the intra-rater errors. Only

white matter around the stem cell implanted foci was drawn in the ROIs to improve serial follow-up consistency. Besides, the size, shape and location of ROIs can be saved in the software and recalled in the follow-up images. Mean perfusion values (rCBV, rCBF) of the ROI were compared with the ROI in the contralateral relative normal white matter (corona radiate) of the same patient. We monitor the longitudinal focal cerebral blood flow and volume change by perfusion ratio. The ratios are calculating as $\frac{\text{rCBF of graft ROI}}{\text{rCBF of contrallateral normal white matter}}$ and $\frac{\text{rCBV of graft ROI}}{\text{rCBV of contrallateral normal white matter}}$ in each scan (Figure 1).

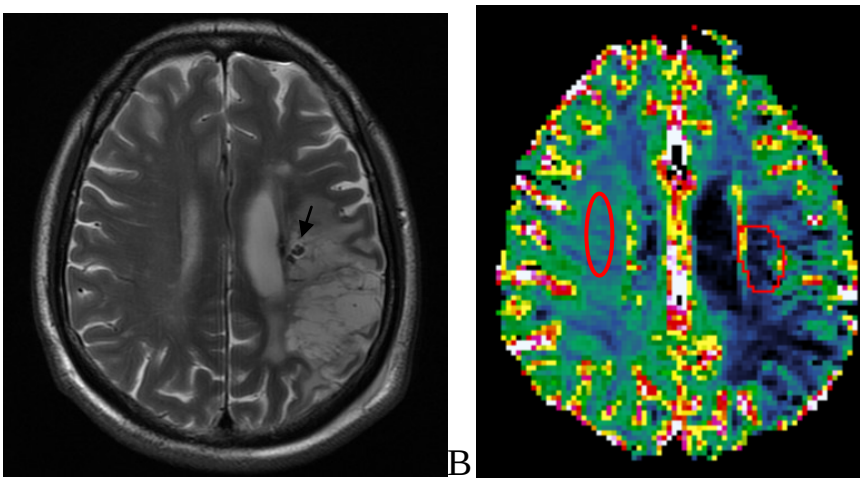

Figure 3.1. Draw the regions of interest on MR perfusion image. A) T2-weighted FSE axial image showed focal hypointensity (arrow) resulted from the SPIO labeled on the stem cells in the peri-infarct area 1-day after implantation. B) The measured ROIs (red circles) showed on the relative blood volume map of MR perfusion study.

We found three lesions resulted by needle tracts with the appearance of small hyperintense holes on one-day follow-up T2W FSE images. The perfusion ratios between the ROIs around the needle tracts and the contralateral normal white matter were measured.

Procedural-related small macroscopic acute hematomas were depicted in 8 patients on one-day follow up. The acute hematoma appeared as hypointense irregular-shaped nodule on FSE T2W axial images and T2W gradient images. For comparison of the perfusion change at the stem-cell injected areas, we also measure the perfusion ratios between the ROIs around the hematoma and the contralateral normal white matter.

NIHSS of the patients

The National Institutes of Health Stroke Scale (NIHSS) of all patients were recorded each time they returned to follow up the MR studies.

Statistical methods

The dependence of flow measures on time was assessed using the Friedman test. When the overall difference among time points was significant, post-hoc analysis with the Wilcoxon signed-rank test was performed with Bonferroni correction. The significance level was chosen to be 0.05.

3.3 Results

Table 3.1 Description of patients

Patient No.	Sex/Age (yr)	Onset of Stroke (mo[#])	Stroke Site	NIHSS (baseline/6mon/12 mon/improved[*])	perfusion group
1	M/44	60	>1/3 left MCA infarction with cavity and hemorrhagic transformation	9/7/7/2	B
2	M/61	48	Lacunar infarct in the left corona radiata	9/9/7/2	A1
3	F/54	37	>1/3 left MCA infarction with cavity, no hemorrhage	9/6/6/3	A1
4	F/31	22	Hemorrhagic infarct in the right putamen and right corona radiata	9/9/5/4	A1
5	F/57	50	Lacunar infarct in the posterior limb of right IC	11/8/3/8	B
6	M/36	39	Small infarct in the left corona radiate (<1/3 left MCAT)	9/4/3/6	B
7	M/65	11	Hemorrhagic infarct in the right putamen, involving posterior limb of right IC	9/4/3/6	B
8	M/51	53	Hemorrhagic infarct in the bilateral putamen, involving left corona radiata	10/6/4/6	A1
9	M/58	36	Hemorrhagic infarct in the left putamen, involving left corona radiata	10/6/5/5	A1
10	M/54	13	Hemorrhagic infarct in the right putamen and right corona radiata, old infarct in the right parietal lobe	11/6/7/4	A2
11	M/47	25	Leukomalacia in the left corona radiata	9/4/4/5	A1
12	M/47	8	Lacunar infarct in the right putamen and posterior limb of right IC	10/8/8/2	B
13	M/47	32	Hemorrhagic infarct in the left putamen, involving left corona radiata	9/8/8/1	A2
14	M/43	7	Hemorrhagic infarct in the right putamen and right corona radiata	9/8/7/2	B
15	M/49	41	Hemorrhagic infarct in the left thalamus and left putamen	9/7/6/3	A2

MCA: middle cerebral artery; IC: corona radiata; MCAT: middle-cerebral-artery territory

#: The interval between the stem cell implantation and the onset of stroke

*: The NIHSS 12 month after implantation- NIHSS score of the baseline

Perfusion around the implanted grafts

We divided the fifteen patients into two groups. Nine patients were in the Group A and six patients in the Group B. The MR perfusion studies in Group A showed significant relative blood flow and volume increase one week (T3) after stem cell implantation as compared to the baselines (T1) (Figure 2). Six patients (Group A-1) in Group A showed still mild increased relative blood flow and volume one month (T4) after stem cell implantation. But the increase amount showed no statistical significance compared with the baseline (T1) (Figure 3). Another three patients (Group A-2) in Group A showed transient severe focal interstitial edema with sharply drop of relative blood flow and volume one month (T4) after stem cell implantation (Figure 4). This resulted in the decreased mean values of relative blood flow and volume at T4 in Group A (Figure 2). In Group B, the relative blood flow and volume did not change significant in the longitudinal follow up (Figure 5).

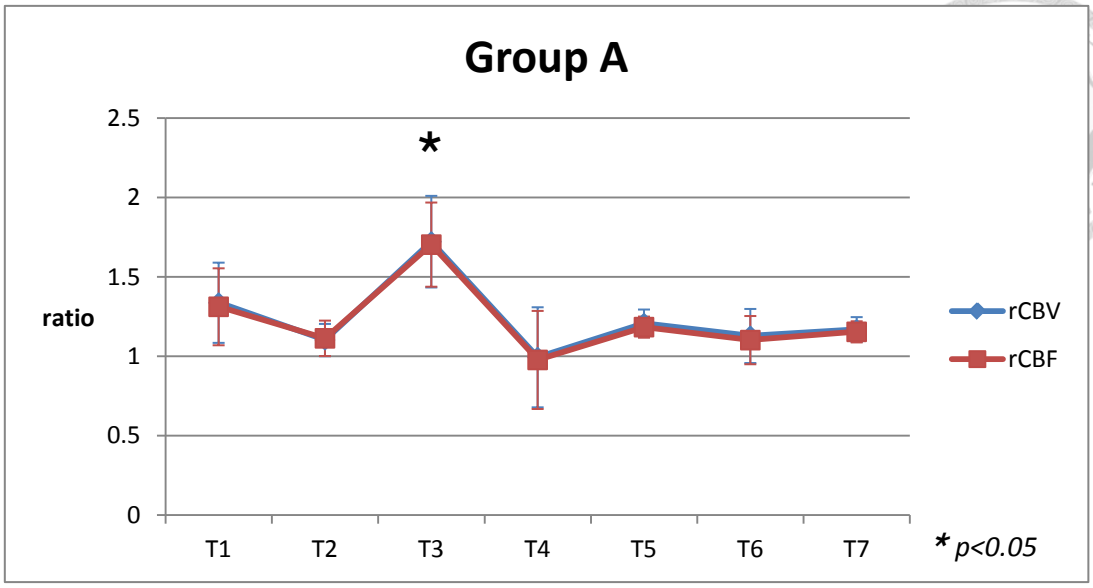

Figure 3.2. Longitudinal perfusion changes in Group A. The perfusion ratio of relative cerebral blood flow and volume increased significantly in the 1-week (T3) follow-up studies of Group A. (T1: the time point before stem cell implantation, T2: one day after stem cell implantation, T3: 1 week, T4: 1 month, T5: 3 months, T6: 6 months, T7: 12 months after stem cell implantation).

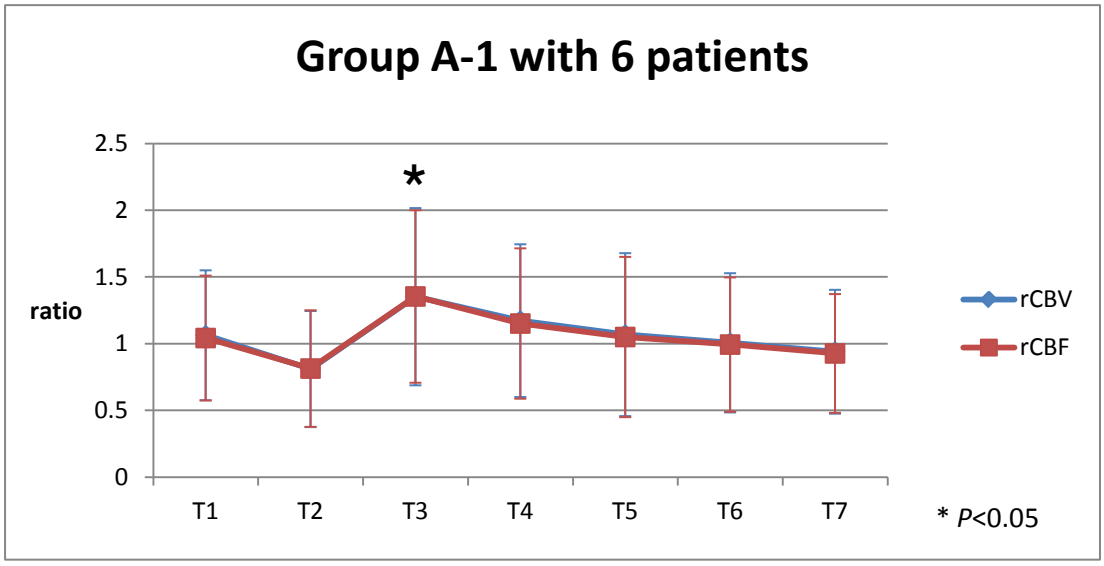

Figure 3.3. Longitudinal perfusion changes in Group A-1. Relative

Cerebral blood volume and flow increased ($p<0.01$) at T3 (one week after stem cell implantation). Mild increased at T4 (one month after stem cell implantation) but without significant statistical differences as compared to T1.

A 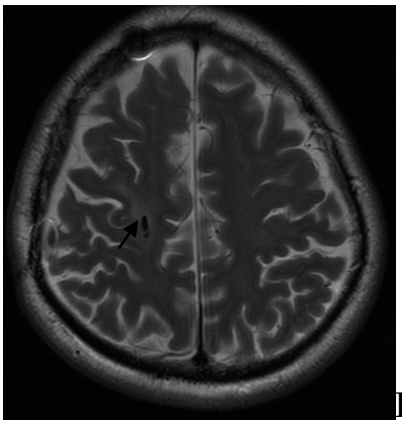 B 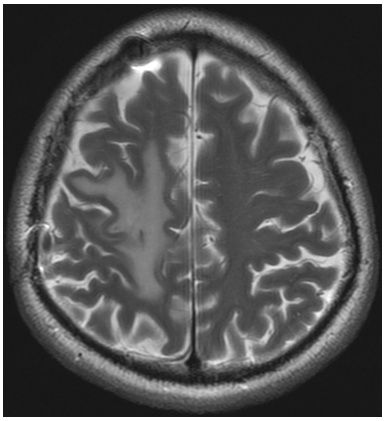

C 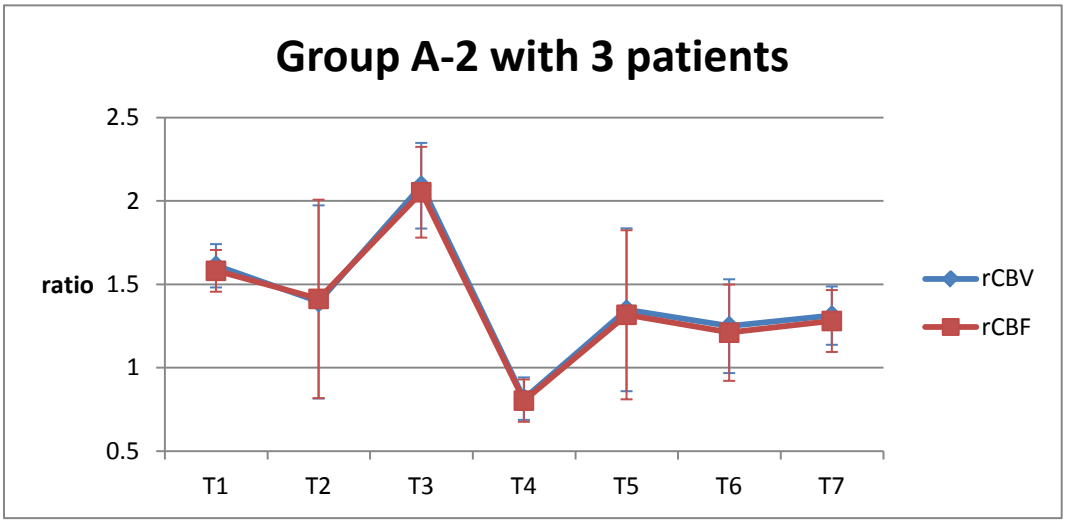

Figure 3.4. Longitudinal perfusion changes in Group A-2. A) Focal hypointensity (arrow) marked the implanted stem cells on 1-day follow-up T2W FSE images. B&C) Transient severe focal interstitial

edema around the implanted site was shown at T4 with decreased cerebral blood volume and flow.

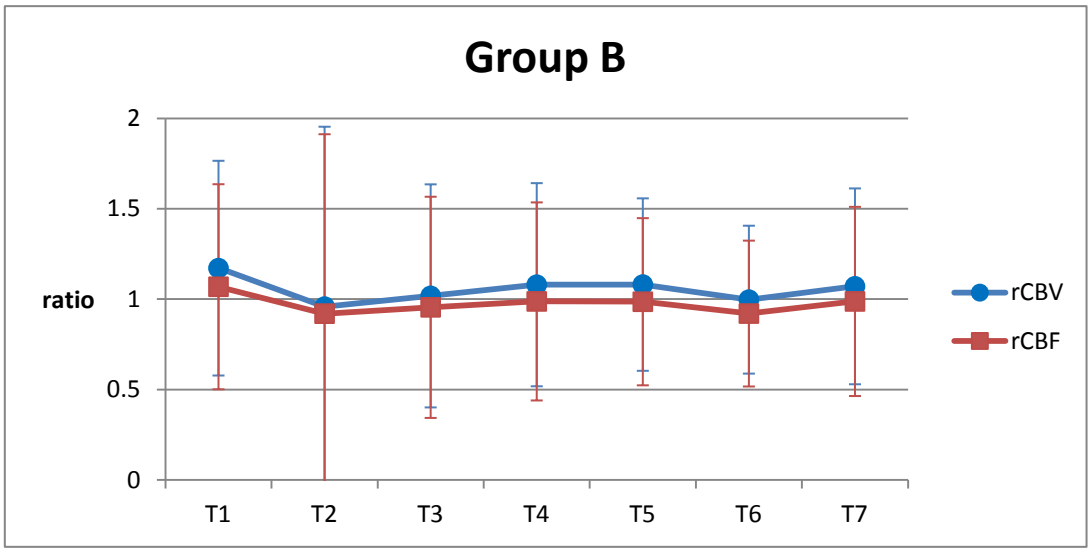

Figure 3.5. Longitudinal perfusion changes in Group B. No significant blood volume and flow change can be detected on the MR perfusion follow ups in Group B patients.

Perfusion around the needle tracts

From analyzing the FSE T2W images and T2W gradient images, three small lesions resulted from the needle insertion were depicted in three patients. The lesions were tiny and round with hyperintense T2W signals. The relative blood flow and volume increased one day (T2) after stem cell implantation and returned to the baseline one week (T3) after stem

cell implantation (Figure 6). The relative blood flow and volume were mild decreased three months after the procedure.

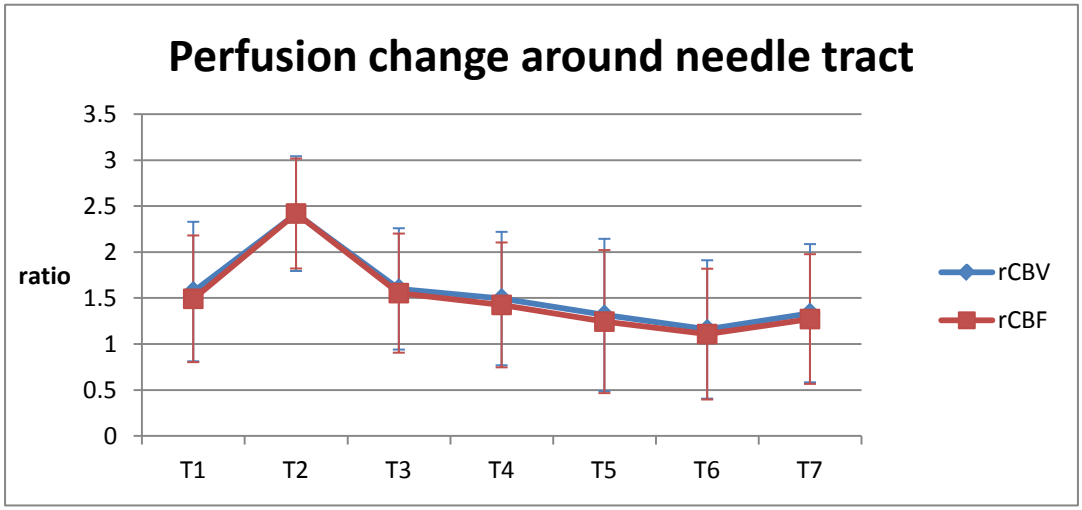

Figure 3.6. Longitudinal perfusion changes around needle tracts. Transient increase of both relative blood flow and volume was shown on the 1-day follow-up MR perfusion study. The rCBV and rCBF returned to the baseline at T3 (1-month follow-up).

Perfusion around the procedural-related acute hematoma

From analyzing the FSE T2W images and T2W gradient images, procedural-related intracerebral acute hematoma were depicted in 8 patients. The relative blood flow and volume around the hematoma decreased from T2 without returning to the baselines thereafter (Figure 7).

A 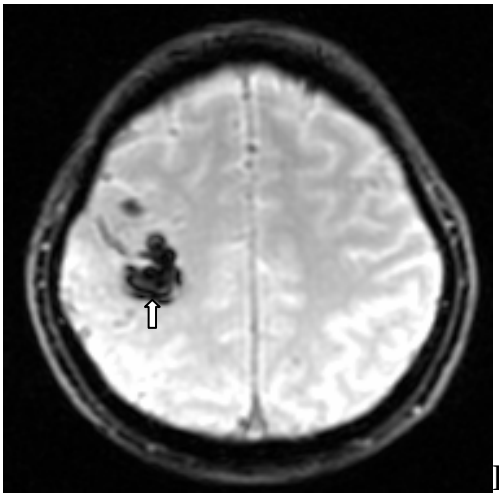 B 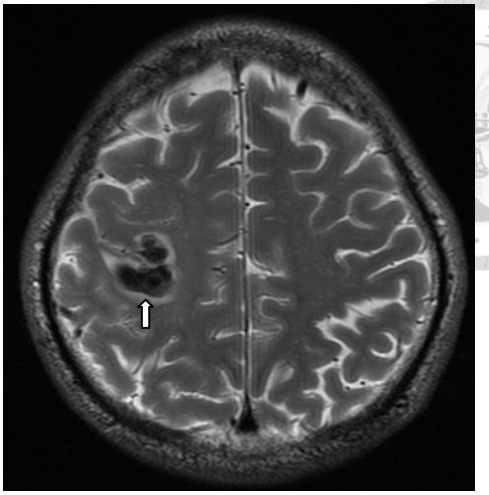

C 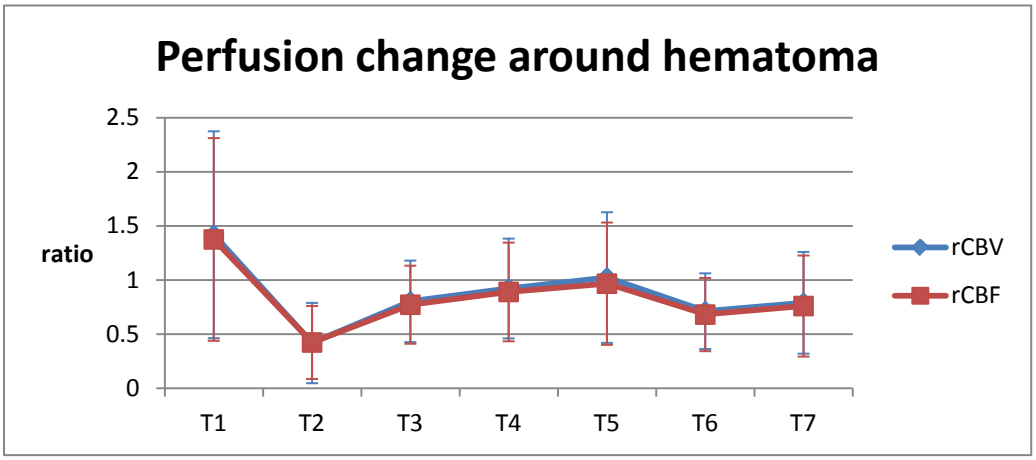

Figure 3.7. Longitudinal perfusion changes around hematoma. The relative blood flow and volume around the hematoma (arrow) decreased from T2 without returning to the baselines thereafter. The products of the blood have paramagnetic or superparamagnetic effects which interferes the local perfusion measurement and resulted in underestimation of local rCBV and rCBF during the 12 month follow up.

Table 3.2 Summary of perfusion changes in different regions of interest (ROIs)

ROIs	**No.**	**Perfusion change (rCBV and rCBF) as compared to baseline (t1)**	**Possible mechanisms**
Group A	9	↑ rCBV and rCBF at t3*(A) ↑ rCBV and rCBF at t4(A1) ↓ rCBV and rCBF at t4(A2)	Angiogenesis[4,6,8,10,13] HAMA response[20-23]
Group B	6	No change	Previous old hematoma and/or Procedural-related hemorrhage result in underestimation
Needle tract	3	↑ rCBV and rCBF at t2	Procedural-related inflammation
Hematoma	8	↓ rCBV and rCBF at t2~t7	Hemoglobin products result in underestimation

NIHSS of the patients

The means of all 15 patients, group A and group B were presented in the Figure 8. The mean NIHSS score before treatment was 9.5 ± 0.7. Patients began to improve neurologic function with decrease NIHSS from T4 (one month after stem cell implantation). The neurologic function gradually improved till one year (T7) after stem cell implantation. The mean NIHSS score one year after cell implantation was 5.5 ± 1.8, with a mean decrease of 4. No significant differences in NIHSS between group A and B was found.

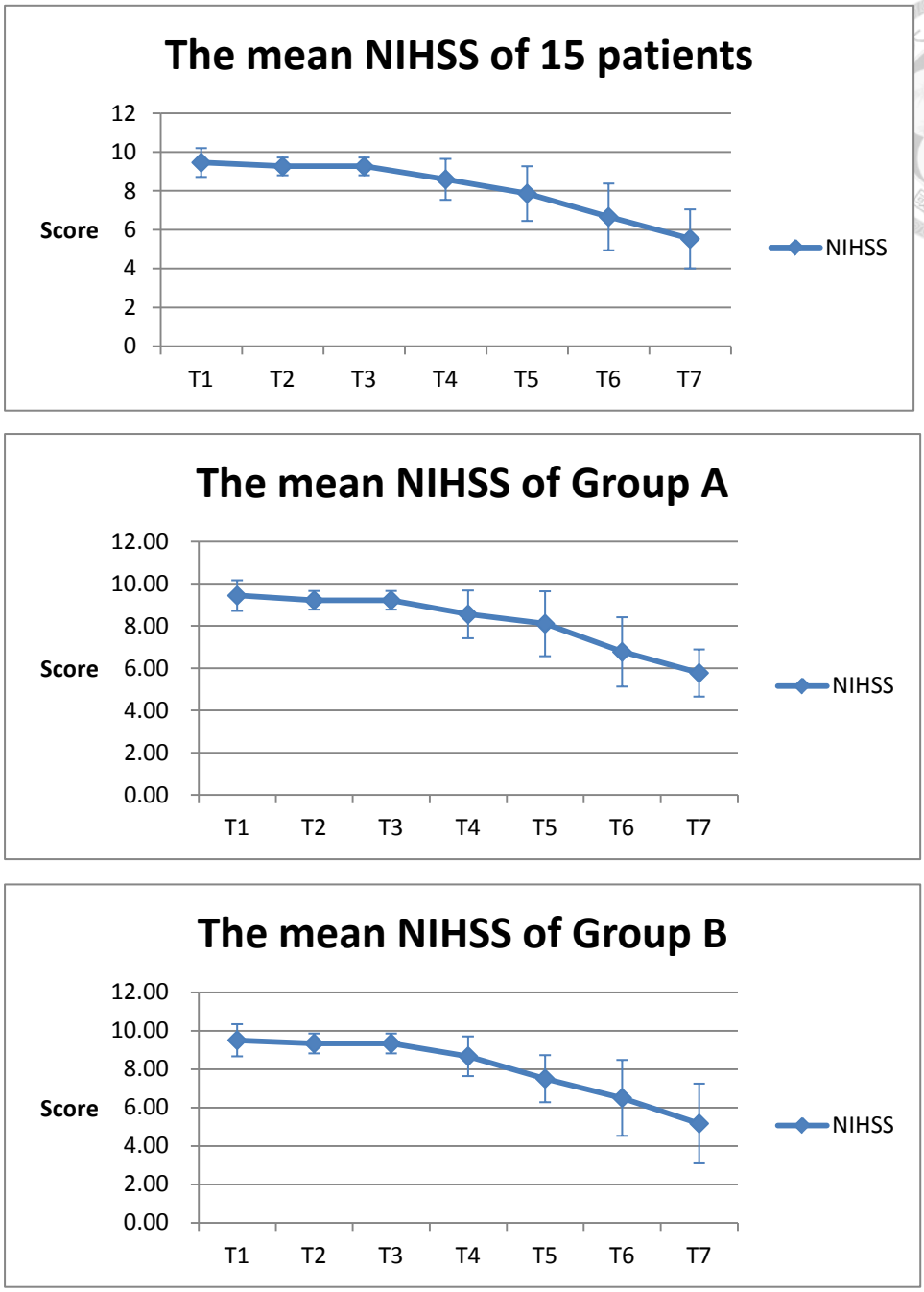

Figure 3.8. The mean and standard deviation of the NIHSS scores in the 15 patients. Patients began to improve neurologic function with decrease NIHSS from T4 (one month after stem cell implantation). The neurologic function gradually improved till one year (T7) after stem cell implantation.

3.4 Discussion

To our knowledge, this is the first trial to investigate longitudinal perfusion change after intracerebral stem cell implantation in chronic stroke patients. Though animal studies have shown angiogenesis after $CD34^+$ implantation by immunostaing (8-9), it's still challenging to survey the perfusion change with MR $T2^*$ perfusion sequence in vivo human brain.

In this study, the stem cells labeled with SPIO were intracerebrally implanted along the lesion-side corticospinal tract with navigation. In Taguchi's study (9), the $CD34^+$ cells were intravenously administered via tail vein 48 hours after stroke. Labeling vasculature by infusion of carbon black ink demonstrated neovasculature at the border of the MCA and ACA cortex in animals treated with CD 34^+ cells on day 7 and day 14. Another animal study by Jiang et al. (11) intracisternally transplanted the subventricular zone cells which were isolated from adult rat 48 hours after stroke. Their MR perfusion data showed a transient, time-dependent increase in *K*i in the angiogenic areas after cell transplantation. The increase in *K*i was in the subcortical region which maximized at 2 weeks and returned to normal at 6 weeks. They also showed a continuous

increase in CBF and CBV in the angiogenic related areas after cell treatment which was confirmed by histology. The increase in CBF and CBV started at 3 weeks and with increased contrast at 6 weeks. The animal study (8) with intracerebral allograft CD 34^+ cell implantation 7 days after stroke showed increased relative cerebral blood flow using LDF monitoring with Diamox injection. The increase in relative cerebral blood flow was significant as compared to the control group with intracerebral saline injection 7 and 14 days after stem cell implantation.

Nine of the 15 patients showed transient increase in relative cerebral blood flow and volume around the stem cell implantation sites which are peri-infarct areas. The increase was significant one week after stem cell implantation as compared to the baseline before stem cell implantation. Quantitative measurement of blood vessel density examined by immunostaining of CD31 showed increased vessel density in the penumbric area of treated rats (8). Furthermore, human $CD34^+$ cell have been shown to secrete numerous angiogenic factors, including VEGF, HGF, and IGF-1(12). Our results are in agreement with the findings of Taguchi (9) and Shyu (8). Taguchi's hypothesis that $CD34^+$ cells may

induces neovascularization n the ischemic zone and provides a favorable environment for neuronal regeneration (9).

The data of 9 patients in Group A have two patterns at T4 (one month after implantation). Six of the 9 patients showed mild increase in relative cerebral blood flow and volume though the difference was not significant statistically as compared to the baseline. This was also consistent with Shyu's animal study which showed mild increase relative cerebral blood flow but without statistical significance in the PBSC-treated rats as compared with control rats 28 days after stem cell implantation.

Three of the 9 patients in Group A showed mild focal interstitial edema at T3. The edema reached maximal involvement at T4 (one month after implantation). This finding was not reported in the animal study. The focal interstitial edema was with complete remission at T5 (3 months after implantation). The injury by the needle was maximal in the one day follow-up MR images. The peri-hemorrhagic edema was maximal within 7 to 11 days after the bleeding event (13); therefore this transient focal edema one month after implantation was less likely resulting by the procedural-related hemorrhage. As for the macrophages loaded with USPIO in animal study, the time course of loading macrophages with

USPIO is 24-72 hours after the injection of USPIO into the blood stream (14). This time course is early than our transient maximal edema at T4. The stem cells are autologous bone marrow transplant; no immunosuppression regimen was applied on the patients after stem cell implantation in this study. The spontaneous development of graft versus host disease (GVHD) following autologous transplantation is rare but has been reported (15-16), arising in 5–10% of cases and occurring more predictably when cyclosporin A is given post-transplant. It is thought to result from a failure of the regenerating immune system to acquire tolerance to self MHC antigens in the post-transplant period, leading to the development of autoreactive T cells. In our study group, 3 of 15 patients (20%) are with transient focal edema. This incidence is much higher than the reported GVHD in autologous transplantation groups and makes GVHD less likely the cause of transient brain edema. Another possible cause is human anti-animal antibody (HAMA) response. A unique aspect of the CliniMACS system is that the antibody conjugate, once bound to the CD34+ cells, is not removed and is then implanted into the patient's brain parenchyma. The antibody conjugate consists of a murine monoclonal antibody (AC101) covalently bound to microbeads

made of an iron–dextran complex (17). Allergic responses to iron–dextran when used as a therapy for anemia are widely reported in the literature (18). Besides, patients (from <1% to 80%) were found to have developed a HAMA response following administration of the antibody (19). The precise mechanism of action is not clear but may be due to a type III immune complex immunopathologic reaction (20). Patients receiving murine antibodies, particularly in high amounts, may form human antibodies against these foreign proteins or HAMA, which usually occur within 2–3 wk after the first mouse antibody administration and within hours or days after a repeated administration(21). The incidence (20%) and onset timing (mild edema in one week and reaching the maximum at 4 weeks) of the transient focal brain edema in our patient group matches that of HAMA response. None of the patients show prominent new neurological deficits related to this transient focal brain edema.

One might criticize that the procedure of intracerebral injection itself may cause damage (22). In animal study (8), intracerebral normal saline injection was performed in the control rats. The blood vessel density was increased in the stem-cell treated rats as compared with control rats. In

this human study, sham control with intracerebral normal saline injection was not allowed by the department of health. Therefore, we analyze the perfusion change resulted by the needle tract and procedural-related hematomas for comparisons. The inflammatory change resulted by the needle injury causes blood flow and volume increase one day after the procedure. This effect lasted shortly and returned near the baseline in the one week follow-up, which is different from the effect by stem cells. The hematoma and its products with paramagnetic and superparamagnetic effects interferes the MR perfusion results. The blood flow and volume around the hematoma cannot be exactly measured and are lower than the baseline from one day to one year follow ups.

Although six of the 15 patients (Group B) did have improvement in NIHSS scores, the MR perfusion study cannot detect blood flow/volume change in the stem cell implanted areas. Jiang's study also found that not all the areas with labeled cells promote angiogenesis (11). There might be two reasons to explain for this. Firstly, the perfusion increase in the peri-infarct area may be obscured by the procedural-related hemorrhage. The procedural-related hemorrhage and the subsequent hemosiderin products can be persist depicted in the injection site on the 12-month

follow up MR studies in our studies. Secondly, the implanted areas may not be suitable for stem cell survival. If only small amount of viable stem cells migrate to areas more suitable for survival, the angiogenesis by the viable stem cells cannot be detected by this study.

Our study has several limitations. Firstly, the relative cerebral blood flow and volume was much different in gray matter and white matter. The mean rCBF in gray matter was 69.7 mL/min/100g and 33.6 mL/min/100g (23). Besides, the gray matter was convoluted. For consistency in longitudinal measurement, we only measured the perfusion change in the peri-infarct white matter and avoided the gray matter to include in our measured ROIs. Therefore, our study cannot detect the perfusion change in the peri-infarct gray matter. Secondly, the perfusion method we used is $T2^{*}$-weighted gradient-echo echo-planar sequence. The superparamagnetic iron oxide labeled on the stem cells influenced local magnetic field which resulted in underestimate of the perfusion change at T2 (one day) and T3 (one month) after stem cell implantation. In the future study, spin-echo echo-planar sequence is suggested to reduce some of the susceptibility effect by SPIO. Thirdly, procedural-related local microhemorrhage is not uncommon (24). The hematoma is paramagnetic

at acute and subacute stages and superparamagnetic at chronic stage (25). If procedural-related micro-hemorrhage exists, our results of perfusion may be underestimated. Fourthly, the patient number in this preliminary study is small. Some image findings may be statistically underestimated due to small sample numbers.

3.5 Conclusion

The results of our study show transient increase cerebral blood flow and volume (1 week to 1 month) which then decrease and are a little lower than the baselines in the chronic stroke patient after autologous $CD34^+$ stem cell implantation. The perfusion change is earlier than the clinical neurologic symptoms improvement which begin from 1 month after stem cell implantation.

3.6 Publication

Conference paper

1. (2012) **Chao-Chun Lin**, Wu-Chung Shen, Yung-Jen Ho, Yu-Chien Lo, Po-Pang Tsai, Chia-Wei Lin, Chiao-Ying Wu, Hing-Chiu Chang, Hsiao-Wen Chung, Woei-Cherng Shyu, Shinn-Zong Lin. **Longitudinal perfusion change after intracranial stem cell implantation in chronic stroke patients.** *in International Society of Magnetic Resonance in Medicine*, 20th Annual Meeting, 5-11 May, 2012, Melbourne, Australia #4624 (Electronic Poster)

References

1. Modo M, Stroemer RP, Tang E, Patel S, Hodges H. Effects of Implantation Site of Stem Cell Grafts on Behavioral Recovery From Stroke Damage. Stroke. 2002;33(9):2270-8.
2. Chen J, Li Y, Wang L, et al. Therapeutic Benefit of Intravenous Administration of Bone Marrow Stromal Cells After Cerebral Ischemia in Rats. Stroke. 2001;32(4):1005-11.
3. Li Y, Chen J, Wang L, Lu M, Chopp M. Treatment of stroke in rat with intracarotid administration of marrow stromal cells. Neurology. 2001;56(12):1666-72.
4. Chen J, Zhang ZG, Li Y, et al. Intravenous Administration of Human Bone Marrow Stromal Cells Induces Angiogenesis in the Ischemic Boundary Zone After Stroke in Rats. Circ Res. 2003;92(6):692-9.
5. Englund U, Bjrklund A, Wictorin K, Lindvall O, Kokaia M. Grafted neural stem cells develop into functional pyramidal neurons and integrate into host cortical circuitry. Proceedings of the National Academy of Sciences of the United States of America. 2002;99(26):17089-94.
6. Zhang ZG, Zhang L, Jiang Q, Chopp M. Bone Marrow-Derived

Endothelial Progenitor Cells Participate in Cerebral Neovascularization After Focal Cerebral Ischemia in the Adult Mouse. Circ Res. 2002;90(3):284-8.

7. Shen LH, Li Y, Chen J, et al. Intracarotid transplantation of bone marrow stromal cells increases axon-myelin remodeling after stroke. Neuroscience. 2006;137(2):393-9.
8. Shyu W-C, Lin S-Z, Chiang M-F, Su C-Y, Li H. Intracerebral Peripheral Blood Stem Cell (CD34+) Implantation Induces Neuroplasticity by Enhancing beta1 Integrin-Mediated Angiogenesis in Chronic Stroke Rats. J Neurosci. 2006;26(13):3444-53.
9. Taguchi A, Soma T, Tanaka H, et al. Administration of CD34+ cells after stroke enhances neurogenesis via angiogenesisin a mouse model. The Journal of Clinical Investigation. 2004;114(3):330-8.
10. Calamante F, Gadian DG, Connelly A. Delay and dispersion effects in dynamic susceptibility contrast MRI: Simulations using singular value decomposition. Magnetic Resonance in Medicine. 2000;44(3):466-73.
11. Jiang Q, Zhang ZG, Ding GL, et al. Investigation of neural progenitor cell induced angiogenesis after embolic stroke in rat using MRI. NeuroImage. 2005;28(3):698-707.

12. Majka M, Janowska-Wieczorek A, Ratajczak J, et al. Numerous growth factors, cytokines, and chemokines are secreted by human CD34+ cells, myeloblasts, erythroblasts, and megakaryoblasts and regulate normal hematopoiesis in an autocrine/paracrine manner. Blood. 2001;97(10):3075-85.
13. Staykov D, Wagner I, Volbers B, et al. Natural Course of Perihemorrhagic Edema After Intracerebral Hemorrhage. Stroke. 2011;42(9):2625-9.
14. Dousset V, Delalande C, Ballarino L, et al. In vivo macrophage activity imaging in the central nervous system detected by magnetic resonance. Magnetic Resonance in Medicine. 1999;41(2):329-33.
15. Byrne JL, Carter GI, Ellis I, Haynes AP, Russell NH. Autologous GVHD following PBSCT, with evidence for a graft-versus-myeloma effect. Bone Marrow Transplantation. 1997;20(6):517-20.
16. Jones R, Hess A, Mann R, et al. INDUCTION OF GRAFT-VERSUS-HOST DISEASE AFTER AUTOLOGOUS BONE MARROW TRANSPLANTATION. The Lancet. 1989;333(8641):754-7.
17. Richel DJ, Johnsen HE, Canon J, et al. Highly purified CD34+ cells

isolated using magnetically activated cell selection provide rapid engraftment following high-dose chemotherapy in breast cancer patients. Bone marrow transplantation. 2000;25(3):243-9.

18. Mamula P, Piccoli DA, Peck SN, Markowitz JE, Baldassano RN. Total Dose Intravenous Infusion of Iron Dextran for Iron-Deficiency Anemia in Children With Inflammatory Bowel Disease. Journal of Pediatric Gastroenterology and Nutrition. 2002;34(3):286-90.
19. Kricka LJ. Human Anti-Animal Antibody Interferences in Immunological Assays. Clinical Chemistry. 1999;45(7):942-56.
20. Klee GG. Human Anti-Mouse Antibodies. Archives of Pathology & Laboratory Medicine. 2000;124(6):921-3.
21. Juweid ME. Radioimmunotherapy of B-Cell Non-Hodgkin's Lymphoma: From Clinical Trials to Clinical Practice. Journal of Nuclear Medicine. 2002;43(11):1507-29.
22. Smith HK, Gavins FNE. The potential of stem cell therapy for stroke: is PISCES the sign? The FASEB Journal. 2012;26(6):2239-52.
23. Rempp KA, Brix G, Wenz F, Becker CR, Gückel F, Lorenz WJ. Quantification of regional cerebral blood flow and volume with dynamic susceptibility contrast-enhanced MR imaging. Radiology.

1994;193(3):637-41.

24. Rad AM, Arbab AS, Iskander ASM, Jiang Q, Soltanian-Zadeh H. Quantification of superparamagnetic iron oxide (SPIO)-labeled cells using MRI. Journal of Magnetic Resonance Imaging. 2007;26(2):366-74.

25. Gomori JM, Grossman RI. Mechanisms responsible for the MR appearance and evolution of intracranial hemorrhage. Radiographics. 1988;8(3):427-40.